SPATIO-TEMPORAL ANALYSIS OF SEISMIC HAZARD POTENTIAL IN THE SOUTHWESTERN REGION OF THE EAST ANATOLIAN FAULT

by

İpek Sarıbaşak

B.S., Geomatics Engineering, Yıldız Technical University, 2014

Submitted to the Kandilli Observatory and Earthquake
Research Institute in partial fulfillment of
the requirements for the degree of
Master of Science

Graduate Program in Geodesy
Boğaziçi University
2025

SPATIO-TEMPORAL ANALYSIS OF SEISMIC HAZARD POTENTIAL IN THE SOUTHWESTERN REGION OF THE EAST ANATOLIAN FAULT

APPROVED BY:

Prof. Haluk Özener (Thesis Supervisor)	. . . .
Assist. Prof. Tülay Kaya Eken	. . . .
Prof. Uğur Doğan Şanlı	. . . . ………

DATE OF APPROVAL: 15/08/2025

ACKNOWLEDGEMENTS

First and foremost, I would like to express my sincere appreciation to Prof. Dr. Haluk Özener, my thesis advisor, for his dedicated mentorship, intellectual input, and continued support at every stage of this research. I am especially thankful for the academic freedom he provided me, which allowed me to explore my ideas during this study. His profound knowledge in geodesy and earthquake science, combined with his patient mentorship and critical perspective, greatly contributed to the development of this study. It has truly been a privilege to work under his supervision.

I would like to express my deepest gratitude to Assist. Prof. Dr. Tülay Kaya Eken for motivation and her immense guidance. Since the beginning of this study, she empowered me to believe in myself and took my hand in every obstacle I encountered. She never withheld her kindly help and invaluable time from me, generously shared her knowledge and experience with me, and I always felt her moral support. I could never end up this study without her endless support. It was a great pleasure to have the opportunity to study with her.

I would like to give my special thanks to Prof. Dr. Semih Ergintav, and Dr. H. Onur Yılmaz for sharing their valuable knowledge throughout my master’s education and to all the faculty members in the KOERI, Geodesy Department, for their sincerity. Special thanks I would like to give to jury members for their valuable contributions.

Last but not the least, I would like to express my heartfelt gratitude to my parents, Their countless sacrifices and unwavering support throughout this journey mean more to me than words can express. I would like to sincerely thank Mısra Gedik for her invaluable support. Her contributions in assisting during critical stages of the research, were extremely helpful. I deeply appreciate everything she has done for me. I would also like to thank Serhun Zoroğlu for his valuable technical support, which was greatly appreciated and contributed to the completion of this work. My special thanks go to Simon Hofmeyer, for his encouragement and moral support. I am truly grateful for his presence and belief in me.

ABSTRACT

SPATIO-TEMPORAL ANALYSIS OF SEISMIC HAZARD POTENTIAL IN THE SOUTHWESTERN REGION OF THE EAST ANATOLIAN FAULT

Türkiye is one of the most seismically active regions in the world due to its location at the intersection of the Eurasian, Arabian, and African tectonic plates. The country's tectonic regime is primarily governed by two major strike-slip fault systems, namely the North Anatolian Fault (NAF) and the East Anatolian Fault (EAF). On February 6, 2023, southeastern Türkiye experienced a devastating earthquake doublet, with moment magnitudes of 7.8 and 7.6, occurring nine hours apart along different segments of the EAF system. These events caused widespread destruction across 11 provinces, affecting millions of people and significantly altering the stress regime of the region. This study investigates the seismic behavior of the southwestern part of the EAF system before and after the 2023 earthquakes to understand the seismic hazard potentials. To achieve this, a combined approach was adopted involving Coulomb stress modeling, b-value analysis, and geodetic deformation assessment. Coulomb stress change calculations were performed to evaluate stress transfer and potential triggering in adjacent fault segments. In addition, the b-values, derived from the Gutenberg-Richter frequency-magnitude relationship, were used to detect spatiotemporal stress accumulation and release zones, with additional sub-period analysis revealing the impact of the 2023 events and background seismicity of the region. To complement these two approaches, coseismic deformation was analyzed using the InSAR technique, observing displacement patterns across the affected region. Additionally, strain rate fields were reviewed from regional GPS data to identify areas of increased tectonic stress. By integrating these geodetic and seismological datasets, the study highlights overlapping regions characterized by high strain accumulation, low b-values, and positive coulomb stress changes. The convergence of these datasets contributes a comprehensive framework for understanding tectonic stress evolution and improving future seismic hazard assessments along the southern and southwestern parts of the EAF system.

ÖZET

DOĞU ANADOLU FAYI GÜNEYBATI BÖLÜMÜNÜN MEKANSAL VE ZAMANSAL SİSMİK TEHLİKE ANALİZİ

Türkiye, Avrasya, Arap ve Afrika tektonik levhalarının kesişim noktasında yer alması nedeniyle dünyanın sismik açıdan en aktif bölgelerinden biridir. Ülkenin tektonik rejimi, başlıca iki büyük doğrultu atımlı fay sistemi olan Kuzey Anadolu Fayı (KAF) ve Doğu Anadolu Fayı (DAF) tarafından belirlenmektedir. 6 Şubat 2023 tarihinde Türkiye'nin güneydoğusunda, DAF boyunca farklı segmentlerde dokuz saat arayla meydana gelen Mw7.8 ve Mw7.6 büyüklüğündeki depremler, 11 ilde büyük yıkıma neden olmuş, milyonlarca insanı etkilemiş ve bölgedeki gerilme rejimini önemli ölçüde değiştirmiştir. Bu çalışma, 2023 depremleri öncesi ve sonrasındaki sismik davranışları analiz ederek bölgedeki deprem tehlikesinin nasıl evrildiğini ortaya koymayı amaçlamaktadır. Bu amaç doğrultusunda, b-değeri analizi, Coulomb gerilme değişimi modellemesi ve jeodezik deformasyon analizi içeren bütünleşik bir yöntem uygulanmıştır. Gutenberg-Richter frekans-büyüklük ilişkisine dayanan b-değeri, mekansal ve zamansal olarak gerilme birikimi ve boşalımı olan bölgelerin belirlenmesinde kullanılmıştır. Ayrıca çalışma dönemi alt zaman dilimlerine ayrılarak 2023 depremlerinin etkisi ve bölgenin arka plan sismisitesi detaylı biçimde incelenmiştir. Bunun yanı sıra, odak mekanizması çözümleri ve kaynak parametreleri kullanılarak Coulomb gerilme değişim hesaplamaları yapılmış, komşu fay segmentlerindeki olası tetiklenmeler değerlendirilmiştir. Bu iki yaklaşımı tamamlamak amacıyla, InSAR tekniği ile meydana gelen yüzey deformasyonları incelenmiştir. Ayrıca, artan tektonik yüklenme bölgelerini belirlemek amacıyla önceki çalışmalarda kullanılan bölgesel GPS verilerinden elde edilen gerinim oranı alanları gözden geçirilmiştir. Bu veri setlerinin entegrasyonu ile bu çalışmada bölgedeki yüksek gerinim birikimi, düşük b-değerleri ve pozitif Coulomb gerilme değişimleri ile karakterize edilen bölgeler vurgulanmıştır. Bu kapsamlı analiz DAF sisteminin güney ve güneybatı segmentleri boyunca tektonik gerilme evriminin anlaşılmasına ve gelecekteki deprem risklerinin değerlendirilmesine katkı sağlamaktadır.

TABLE OF CONTENTS

LIST OF FIGURES

LIST OF TABLES

LIST OF SYMBOLS

a	A-value
b	B-value
GPa	Gigapascal
M	Magnitude
Mw	Moment Magnitude
$\overline{M}$	The mean magnitude
Mc	Magnitude of Completeness
N (M)	The number of Earthquakes with magnitude ≥ M
Vp	Primary, P-wave Velocity
Vs	Secondary (Shear), S-wave Velocity
ΔCFS	The Coulomb Stress Change
ΔM	The Magnitude Interval
$\Delta\tau$	The Change in Shear Stress
μ'	The Coefficient of Friction
σ_n	The Change in Normal Stress
φ_{int}	The phase of interferogram
φ_{topo}	The phase of topographic height differences
φ_{def}	The phase of ground deformation
φ_{orb}	The phase of orbit inaccuracies
φ_{atm}	The phase of atmospheric delay
φ_{noise}	The phase of temporal and spatial correlation

LIST OF ACRONYMS/ABBREVIATIONS

AFAD	Afet ve Acil Durum Yönetimi Başkanlığı / Disaster and Emergency Management Presidency
AFS	Amanos Fault Segment
AFZ	Antakya Fault Segment
ÇFS	Çardak Fault Segment
ÇOFS	Çokak Fault Segment
DAF	Doğu Anadolu Fayı
E	East
EAF	East Anatolian Fault
EFZ	Engizek Fault Zone
EFS	Erzin Fault Segment
ERFS	Erkenek Fault Segment
DEM	Digital Elevation Model
DIFS	Düziçi-İskenderun Fault Segment
DSF	Dead Sea Fault
FMD	The Frequency-Magnitude Distribution
GPS	Global Positioning System
GR	The Gutenberg-Richter Law
GRB	Göksun Releasing Bend
InSAR	Interferometric Synthetic Aparture Radar
ISCE	InSAR Scientific Compution Environment
KFS	Karataş Fault Segment
KOERI	Kandilli Observatory and Earthquake Research Institute
km	Kilometer
Mc	Magnitude of Completeness
MFZ	Maraş Fault Zone
mm	Millimeter
ML	The Maximum-Likelihood
N	North

NAF	North Anatolian Fault
NE	Northeast
NF	Narlı Fault
NHC	Nurhak Fault Complex
NW	Northwest
SFS	Savrun Fault Segment
SW	Southwest
PAFS	Pazarcık Fault Segment
PFS	Payas Fault Segment
PÜFS	Pütürge Fault Segment
SAR	Synthetic Aparture Radar
SFS	Savrun Fault Segment
SMF	Sürgü-Misis Fault System
SÜFS	Sürgü Fault Segment
TOFS	Toprakkale Fault Segment
TOPS	Terrain Observation with Progressive Scans
W	West
yr	Year
YAFS	Yakapınar Fault Segment
YEFS	Yesemek Fault Segment
YFS	Yumurtalık Fault Segment

1. INTRODUCTION

Türkiye is one of the most tectonically active regions in the world due to its location at the intersection of major tectonic plates (McKenzie, 1972). It is dominated by two major transform fault systems namely, the North Anatolian Fault (NAF) system and the East Anatolian Fault (EAF) system (Figure 1). The NAF is a right-lateral fault system extending for ~1200 km with an east-west striking trend along the Eurasian and Anatolian Plate boundary. It starts from Karlıova in the east and continues towards the North Aegean Sea in the west (Şengör, 1979; Şengör and Canitez, 1982). In contrast, the EAF is a left-lateral fault system extending for ~700 km with a northeast-southwest striking trend along the boundary between Anatolian and Arabian plates (Arpat and Şaroglu, 1972; Arpat and Şaroglu, 1975; Hempton, 1981).

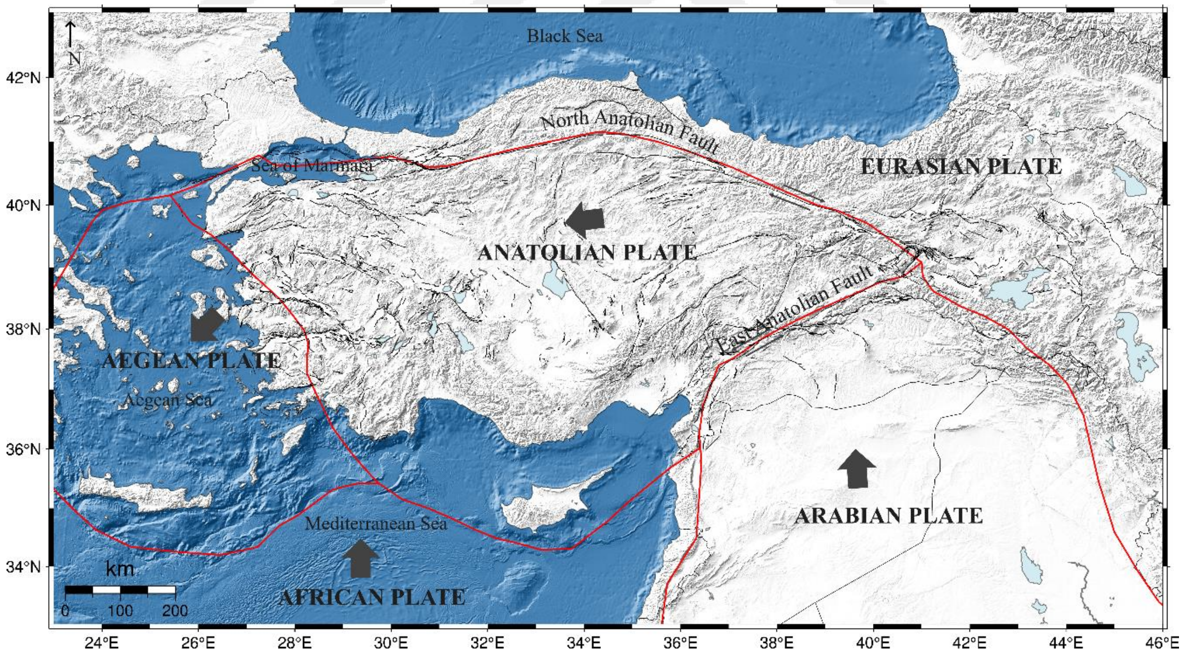

Figure 1.1. The basic tectonic settings of Türkiye. Active faults are illustrated in black lines (Emre et al., 2013). Red line represents the plate boundary (Bird, 2003). The black arrows show the relative motion of tectonic plates.

Türkiye has been highly susceptible to major earthquakes throughout its history. Both the NAF and the EAF have experienced devastating earthquakes over the past 100 years. The NAF, in particular, has been the site of several destructive events during the twentieth century, including the 1912 moment magnitude (Mw) 7.2 Ganos Earthquake, the 1939 Mw 7.8 Erzincan Earthquake, the 1999 Mw 7.4 İzmit and Mw 7.2 Düzce Earthquakes. On the EAF, three moderate events occurred in the last 50 years including the 1971 Mw 6.7, the 2020 Mw 6.1, and the 2020 Mw 6.8 earthquakes. These were followed by two large events, namely the 2023 Mw 7.8 (The Pazarcık Earthquake) and Mw 7.6 (The Elbistan Earthquake) Kahramanmaraş earthquakes.

In February 2023, two devastating earthquakes struck southeastern Türkiye. The first event, with a magnitude of Mw 7.8, took place at 01:17 UTC and was followed just nine hours later by a second shock with a magnitude of Mw 7.6 (KOERI, 2023). This earthquake doublet caused immense destruction and loss of life, impacting a total of 11 provinces in the southern and eastern parts of the country and affecting a combined population of approximately 15 million people (AFAD, 2023). Both earthquakes took place along different fault segments of the EAF system. Based on space geodetic and seismological techniques, both events were characterized by the sinistral strike-slip motion. The first shock ruptured several segments, extending over 300 km in a northeast-southeast direction, while the second shock occurred approximately 95 km northwest of the first event, followed an east-west orientation, and produced a surface rupture of around 150 km. The maximum coseismic slip ranges from 8 to 10 meters for the Mw 7.8 earthquake while for the Mw 7.6 earthquake it ranges from 6 to 12 meters (Melgar et al., 2023; Barbot et al., 2023; Mai et al., 2023; He et al., 2023).

Previous studies have primarily focused on the main fault segments along the EAF, with comparatively less attention paid to secondary or subsidiary fault structures following the 2023 Kahramanmaraş earthquakes. However, the 2023 doublet earthquakes did not occur along the primary strands of the EAF. It demonstrates the importance of reconsidering the role of sub-faults in regional seismic hazard assessments. These faults may still pose significant earthquake risk and should not be underestimated, particularly considering the 2023 earthquakes, which emphasize the importance of monitoring how and where stress is transferred along these structures. Due to the limited number of studies specifically targeting the southern and southwestern segments of the EAF, further investigation is essential to improve the understanding of seismic hazard in these less-studied areas.

This study investigates the seismicity patterns before and after the 2023 doublet earthquakes to identify regions with increased seismic hazard and assess the potential for future earthquake activity along the southern part of the EAF and adjacent fault systems. To achieve this, a multidisciplinary approach was employed; incorporating long-term spatiotemporal b-value analysis and Coulomb Stress change modeling to evaluate variations in crustal stress. Additionally, the Interferometric Synthetic Aperture Radar (InSAR) technique was utilized to detect coseismic surface displacements resulting from the 2023 events. Strain rate fields were also reviewed to identify areas of elevated tectonic loading along the EAF.

The research was conducted in five main steps. First, earthquake catalogs from both historical and instrumental periods were compiled to identify active faults with the potential to generate earthquakes in the region. Focal mechanism solutions were investigated to characterize the faulting mechanism in the region. In the second step, Coulomb stress analysis was applied to further interpret the effects of the doublet earthquakes, demonstrating the redistribution of tectonic stress and the potential for future earthquake triggering within the study region. In the third step, b-values, derived from the Gutenberg-Richter frequency-magnitude relationship, were assessed both spatially and temporally for the period 1995-2024. The analysis was also subdivided into intervals to evaluate variations of b-values over time. In the next step, InSAR analysis was performed to observe deformation resulting from the 2023 doublet earthquakes. In the final step, strain rate fields were reviewed to compare the highlighted regions and to identify areas of increased tectonic loading. The results of this integrated, multidisciplinary approach will provide a framework for improved seismic hazard assessment and contribute to ongoing studies to address earthquake risk in the region.

2. TECTONIC SETTINGS OF THE EAF

2.1. Study Area

The study area is located in the southern and southwestern part of the EAF and it is bounded by latitudes 36.5°N-38.5°N and longitudes 34.5°E-38.5°E (Figure 2.1). This region hold particular importance due to the occurrence of a devastating doublet earthquake sequence in 2023. Additionally, it is located within a tectonically complex zone by the interactions of major plates, making it a critical area for seismic studies.

Approximately 15% of the energy released by global seismic events comes from the Alpide-Himalayan seismic belt, the second most active region in the world after the Ring of Fire (Donner et al. 2010). It is driven by ongoing tectonic deformation occurring within the plates (Console et al. 2003). The belt is located where the Eurasian Plate meets with three major tectonic plates: the African, Arabian, and Indo-Australian Plates (Bird, 2003). Positioned between the Eurasian, Arabian, and African plates, the Anatolian plate forms a small microplate (Figure 1). The formation of this region was shaped by several major tectonic processes, including the closure of the Neotethys Ocean, the collision of the Arabian and African plates with the Eurasian plate to the east, and the subduction of the African Plate in the southwest (Ketin, 1966; Şengör and Yılmaz, 1981; Okay and Tüysüz, 1999; Bozkurt, 2001). These interactions have shaped the region's present-day tectonic setting, leading to various active tectonic zones such as subduction, crustal extension, lateral extrusion, continental collision and escape tectonics. For example, the formation of the EAF and NAF is closely related to the mechanics of escape tectonics in a continental collision setting. (McKenzie, 1972, 1978; Şengör and Yılmaz, 1981; Jackson and McKenzie, 1984; Şengör, 1980; Şengör et al., 1985, Dewey et al., 1986; Barka and Reilinger, 1997; Bozkurt, 2001; Koçyiğit and Özacar, 2003). Due to the complex tectonic framework of Türkiye, it is one of the most geologically active regions in the world.

The EAF is the active tectonic structure in the study area. In the northeast, the EAF extends to Karlıova Basin, where the relative motion between the Eurasian and Arabian plate is accommodated by the NAF, EAF and Varto Fault (Şengör, 1979; Şengör et al., 1985; Şaroğlu, 1985). However, termination of the EAF in the southeast remains a subject of scientific debate. The main fault strand extends in the direction of Cyprus, at the intersection of the Anatolian and African plates based on preliminary research on the EAF (McKenzie, 1972; Dewey, 1973). According to several studies, Kahramanmaraş triple junction, close to Türkoğlu, is where the EAF intersects with the Dead Sea Fault (DSF) (Jackson and McKenzie, 1984; Hempton, 1987, Barka and Kadinsky-Cade, 1988). Other studies argued that in the region between Hatay, Osmaniye and Cilicia, the EAF ultimately connects with the DSF in the southwest. (Arpat and Şaroğlu, 1975; Chorowicz et al., 1994; Duman and Emre, 2013; Şengör et al., 2019). Duman and Emre (2013) convention was followed for the fault names along the EAF in the study area (Figure 2.1).

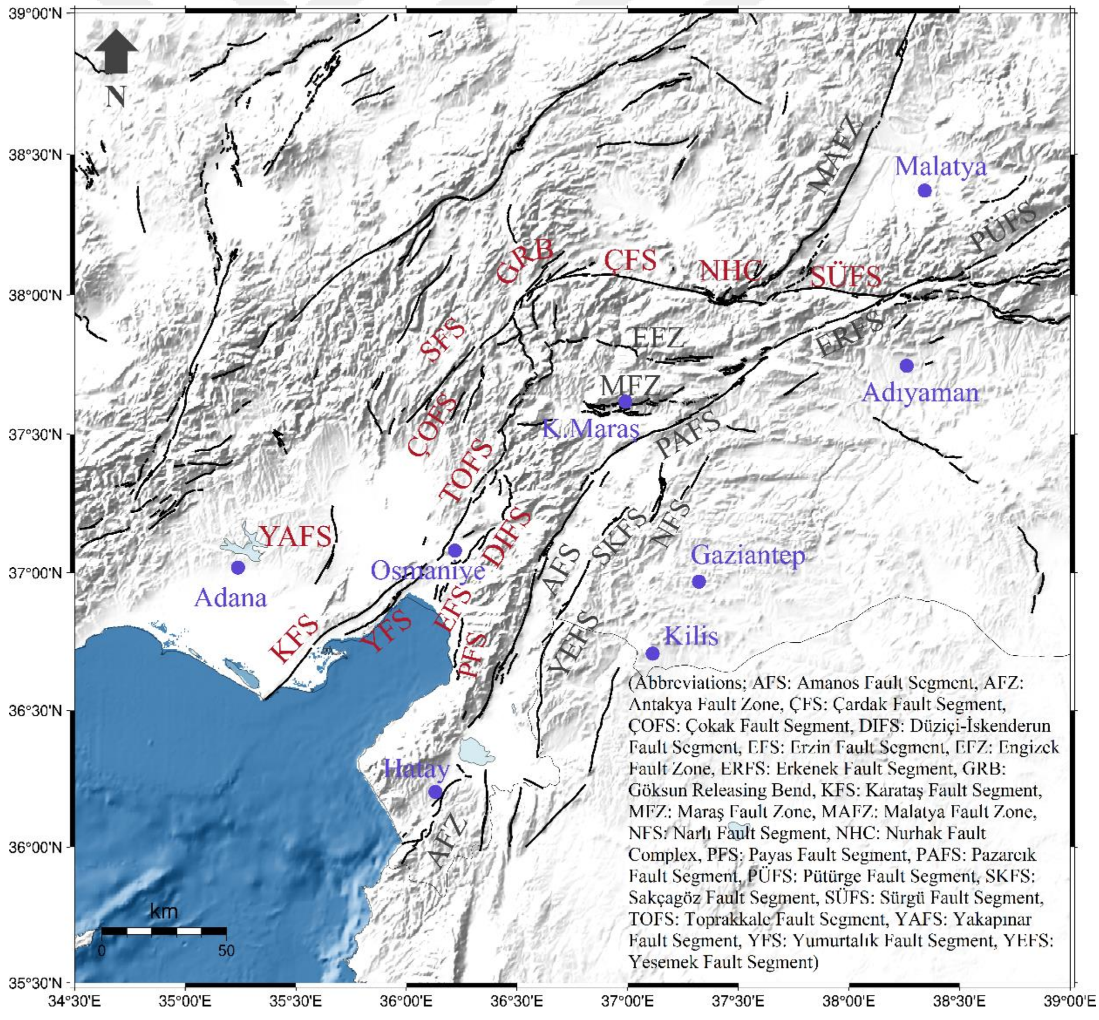

Figure 2.1. Active Faults within the study area along the EAF. Fault names shown in red represent the northern strand of the EAF (Duman and Emre, 2013).

According to Duman and Emre (2013) convention, the EAF is described as comprising two major strands: the main and northern strands. The former, also known as the southern strand, is an active left-lateral fault system that stretches around 580 km from Karlıova to Antakya in the south. The following describes its seven fault segments, which extend from NE to SW (Duman and Emre, 2013):

(i) The Karlıova Fault Segment is a N50°E striking with the length of 31 km.
(ii) The Ilıca Fault Segment is a N40°E striking fault, 40 km long.
(iii) The Palu Fault Segment is a N62°E striking with the length of 70 km.
(iv) The Pütürge Fault Segment is a N60°E striking fault and it is 96 km long.
(v) The Erkenek Fault Segment strikes N75°E and extends for 62 km.
(vi) The Pazarcık Fault Segment is a N60°E striking fault, 82 km long.
(vii) The Amanos Fault Segment is a N35°E trending with the length of 112 km.

The northern strand of the EAF is a 380-km-long active left-lateral strike-slip fault system. It is also known as the Sürgü-Misis Fault System (SMF). It splits from Çelikhan and extends southward to the Gulf of Iskenderun. The following describes nine fault segments of the system (Duman and Emre, 2013):

(i) The Sürgü Fault Segment (SÜFS) is an E-W striking, 55 km-long fault that splits from the EAF near Çelikhan and ends within the Nurhak Fault complex (NHC).
(ii) The Çardak Fault Segment (ÇFS) is an E-W (N75°E) striking, 85 km-long fault located between the NHC and the Göksun bend. It represents as the longest segment of the system.
(iii) The Savrun Fault Segment (SFS) is a N50°E striking fault and it extends for 60 km.
(iv) The Çokak Fault Segment (ÇOFS) is a N15°E striking fault and it is 25 km long.
(v) The Toprakkale Fault Segment (TOFS) strikes N30°-35°E and extends for 52 km.
(vi) The Yakapınar (Misis) Fault Segment (YAFS) is a N45°E trending fault with the length of 35 km.

(vii) The Yumurtalık Fault Segment (YFS) strikes N45°E and extends for 41 km.

(viii) The Karataş Fault Segment (KFS) is a N41°E striking fault with a length of 64 km.

(ix) The Düziçi-Iskenderun Fault zone consists of three fault segments: The Düziçi-İskenderun (DIFS), Erzin (EFS), and Payas (PFS) segments. The Düziçi-İskenderun strikes NE-SW and extends for 45 km. The Erzin comprises parallel faults trending N15°-20°E. The Payas is a 26 km-long fault striking N10°E and dipping 65°-70° to the west.

Geodetic observations (Figure 2.2) suggested that Anatolia microplate and neighboring regions are rotating counterclockwise and displacing in a southwest direction with respect to Eurasia (McClusky et al., 2000; Reilinger et al., 2006; Aktuğ et al., 2013). According to Reilinger et al. (2006), Arabian and African plates are moving N and NW at slip rates of 15 and 5 mm/yr, whereas the Anatolian and Aegean plate motions with regard to the Eurasian plate are W and SW directions at slip rates of 21 and 33 mm/yr, respectively. Based on previous geological, geodetic, and geomorphological studies, slip rates vary along segments of the EAF (McClusky, 2000; Reilinger et al., 2006; Yılmaz et al., 2006; Mahmoud et al., 2013). Near Karlıova, the slip rate drops from 10 mm/yr to about 4 mm/yr near Türkoğlu (Koç and Kaymakçı, 2013; Bayrak et al., 2015; Aktuğ et al., 2016). Further south, the slip rate reaches about 4.2 mm/yr along the DSF's northern segment (Aktuğ et al., 2016; Yıldız et al., 2020). Along the northern strand of the EAF, slip rates relatively low and range between 2.5 mm/yr and 1 mm/yr (Duman and Emre, 2013; Yönlü et al., 2017).

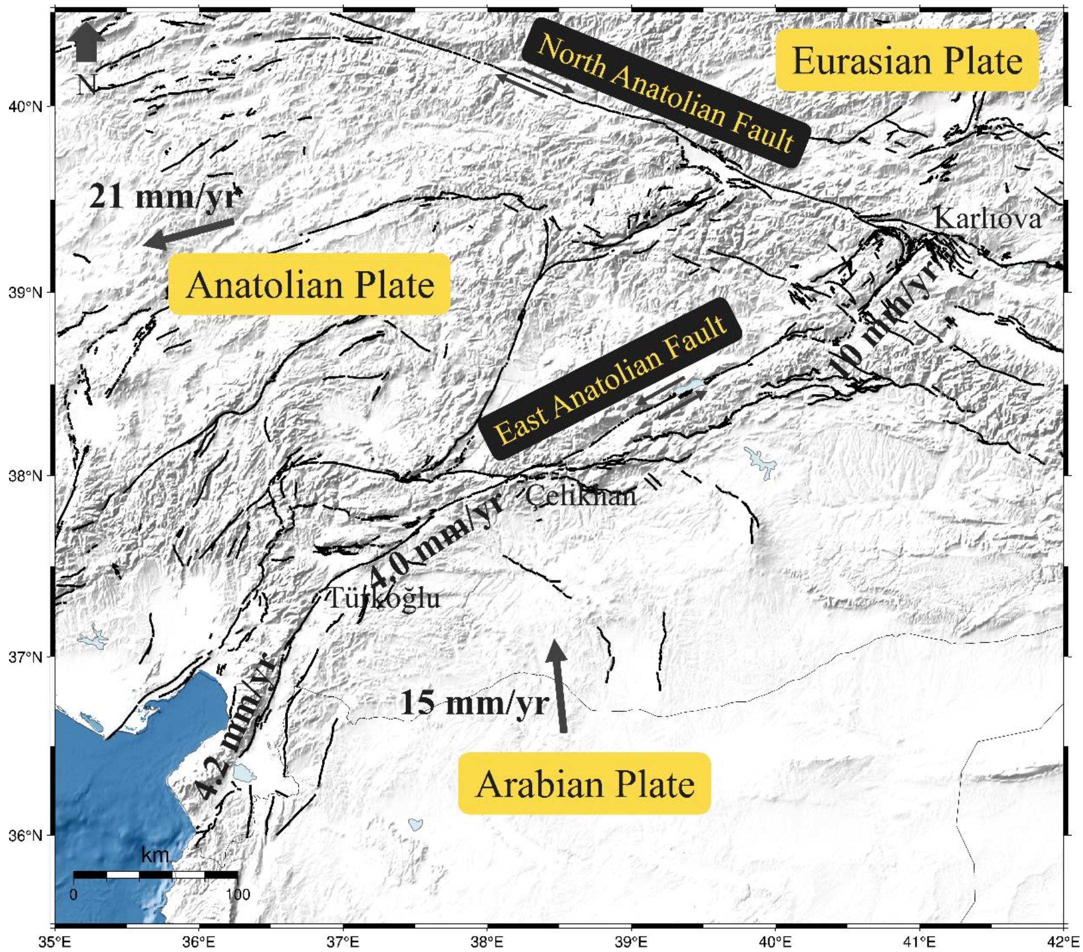

Figure 2.2. Geodetic slip rates of the EAF and the surrounding tectonic plates (modified from Reilinger et al., (2006); Mahmoud et al., (2013); Aktuğ et al., (2016); Yıldız et al., (2020)).

2.2. Present Day and Historical Seismicity

Historical and instrumental period earthquakes that took place in the region were analyzed in order to identify seismic activity in the study area. Historical earthquake catalogs provide long-term data on past earthquakes, with records dating from ancient times to the early 1900's. Historical seismicity helps to assess seismic hazard potential and understand fault behavior over long time. The Disaster and Emergency Management Presidency (AFAD) and the Kandilli Observatory and Earthquake Research Institute (KOERI) data were utilized to compile historical earthquakes that occurred before 1900 within their intensities range of VI-X (Table 2.1).

Table 2.1. List of historical earthquakes.

Year	Longitude	Latitude	Intensity	Reference
679	37,51	36,37	9	AFAD
713	37,96	36,53	8	AFAD
715	37,9	36,5	9	AFAD
791	37,1	36,2	8	AFAD
963	37	36,6	8	AFAD
1003	37,51	36,37	8	AFAD
1037	37,51	36,37	7	AFAD
1042	37,9	36,5	8	AFAD
1089	37,9	36,5	8	AFAD
1109	37,9	36,5	8	AFAD
1114	35,5	36,5	7	AFAD
1137	37,15	36,2	9	AFAD
1138	37,2	36,3	8	AFAD
1156	37,15	36,21	8	AFAD
1204	37,1	36,2	8	AFAD
1404	37	36,3	7	AFAD
1854	36,6	36,2	7	AFAD
1719	37,1	36,2	9	AFAD
1779	37,15	36,21	5	AFAD
1795	37,1	36,2	7	AFAD
1831	37,1	36,2	7	AFAD
1846	37,1	36,2	6	AFAD
1884	37,2	36,3	7	AFAD
1873	35,9	36,1	6	AFAD
37	36,1	36,24	8	AFAD
41	36,17	36,12	8	AFAD
79	36,1	36,25	7	AFAD
115	36,1	36,25	9	AFAD
117	36,1	36,25	7	AFAD
220	36,1	36,25	8	AFAD
240	38,25	38,32	9	AFAD
242	36,5	37,3	10	AFAD
272	36,1	36,25	8	AFAD
300	35,8	37,06	8	AFAD
341	36,1	36,25	8	AFAD
345	36,1	36,25	8	AFAD
388	36,1	36,25	6	AFAD
395	36,1	36,25	8	AFAD
458	36,1	36,25	9	AFAD
506	36,1	36,25	9	AFAD
525	35,9	37,2	8	AFAD

Table 2.1. List of historical earthquakes. (cont.)

Year	Longitude	Latitude	Intensity	Reference
525	36,49	36,7	6	AFAD
526	36,1	36,25	9	AFAD
526	36,1	36,25	6	AFAD
527	36,1	36,25	6	AFAD
528	36,1	36,25	9	AFAD
553	36,1	36,25	7	AFAD
557	36,16	36,2	7	AFAD
558	35,9	37,2	8	AFAD
570	36,17	36,19	8	AFAD
577	36,17	36,18	7	AFAD
579	36,1	36,25	7	AFAD
581	36,1	36,25	6	AFAD
588	36,1	36,25	9	AFAD
639	36,1	36,25	7	AFAD
716	36,1	36,25	7	AFAD
775	36,1	36,25	7	AFAD
803	34,9	36,91	8	AFAD
860	36,1	36,25	9	AFAD
867	36,1	36,25	9	AFAD
952	36,93	37,58	7	AFAD
972	36,1	36,25	7	AFAD
1053	36,1	36,25	8	AFAD
1091	36,1	36,25	7	AFAD
1114	36,1	36,25	8	AFAD
1114	36,9	37,6	9	AFAD
1190	36,1	36,25	8	AFAD
1212	36,1	36,25	6	AFAD
1222	37,1	36,74	6	AFAD
1407	36,48	36,7	6	AFAD
1537	36,16	36,2	6	AFAD
1544	37	38	8	AFAD
1726	36,1	36,25	6	AFAD
1738	36,1	36,25	7	AFAD
1779	38,3	38,35	8	AFAD
1822	36,2	36,4	9	AFAD
1738	36,1	36,25	7	AFAD
1779	38,3	38,35	8	AFAD
1822	36,2	36,4	9	AFAD
1872	36,5	36,4	10	AFAD
1872	36,5	36,4	6	AFAD
1875	36,1	36,2	7	AFAD

Table 2.1. List of historical earthquakes. (cont.)

Year	Longitude	Latitude	Intensity	Reference
1890	38,3	38,35	6	AFAD
1893	37,24	37,03	9	AFAD
1895	38,3	38,4	6	AFAD
1896	35,3	37	6	AFAD
1114	35,5	36,5	9	KOERI
1268	35,5	37,35	9	KOERI

As seen in the Figure 2.3, there are earthquakes around Cilicia Region and Hatay city. Due to the historical significance of its ancient cities, many of these events were likely well-documented by local churches in the region. The AD 242 and the AD 1872 earthquakes were the most destructive earthquakes in the study area, both reaching an intensity of X. According to Duman et al. (2020), the SMF fault system was investigated using paleoseismological trenches. They identified the AD 242 earthquake in their trenches along the Karataş, Yumurtalık, and Osmaniye faults. Their findings suggested that this event ruptured multiple segments in the region. Unfortunately, only a few events have been recorded on the northern strand of the EAF throughout the past two millennia, which is not sufficient to understand the earthquake cycle along the fault segments.

The instrumental seismicity catalogs were obtained from KOERI from January, 1900 to December, 2024 in the study region. The dataset contains 851 events with magnitudes ranging from 4.0 to 7.8. Within the study area, eight earthquakes with magnitudes of Mw >6.0 were observed. These events include the 1907 Niğde (Ulukışla) the 1908 Adana (Işıklı-Kozan) earthquakes, the 1945 Adana (Tatlıkuyu-Ceyhan) earthquake, the 1998 Adana (Hasanbeyli-Sarıçam) earthquake and two devastating earthquakes in 2023 with magnitudes of 7.8 and 7.6, which were followed by significant aftershocks: a Mw 6.6 earthquake in Nurdağı, a Mw 6.0 earthquake in Göksun, and a Mw 6.4 earthquake in Hatay (Figure 2.4).

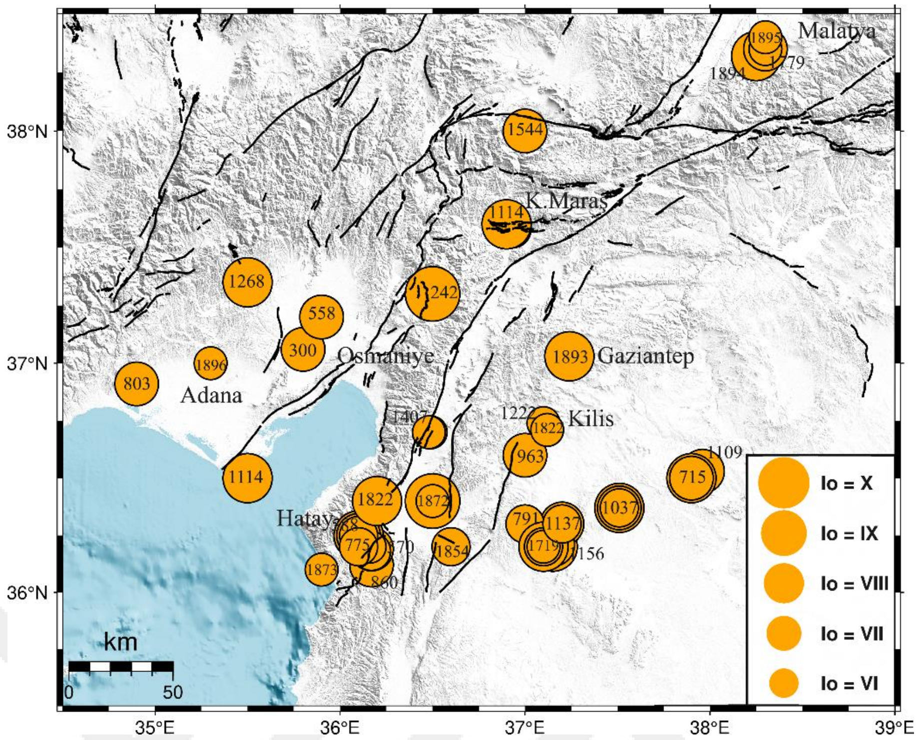

Figure 2.3. Historical seismicity of the study area. When multiple earthquakes took place at the same site, the date of the most recent and largest event is shown.

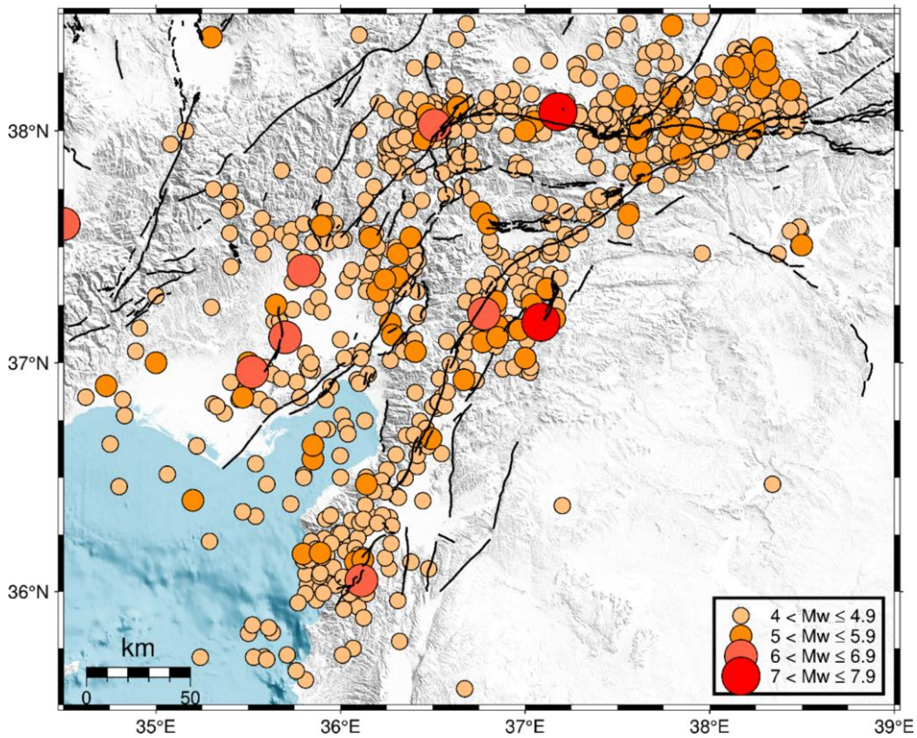

Figure 2.4. The instrumental period earthquakes between 1900 and 2024.

2.3. Focal Mechanisms

The fault plane solutions, derived from AFAD for events with magnitudes larger than 4.0 following the 2023 doublet earthquakes, locally confirm left-lateral strike-slip mechanism of the main strand of the EAF also normal faulting in the south (Figure 2.5). Earthquake focal mechanism solutions of the northern strand of the EAF show strike-slip, normal, and reverse faulting, indicating a complex faulting behavior.

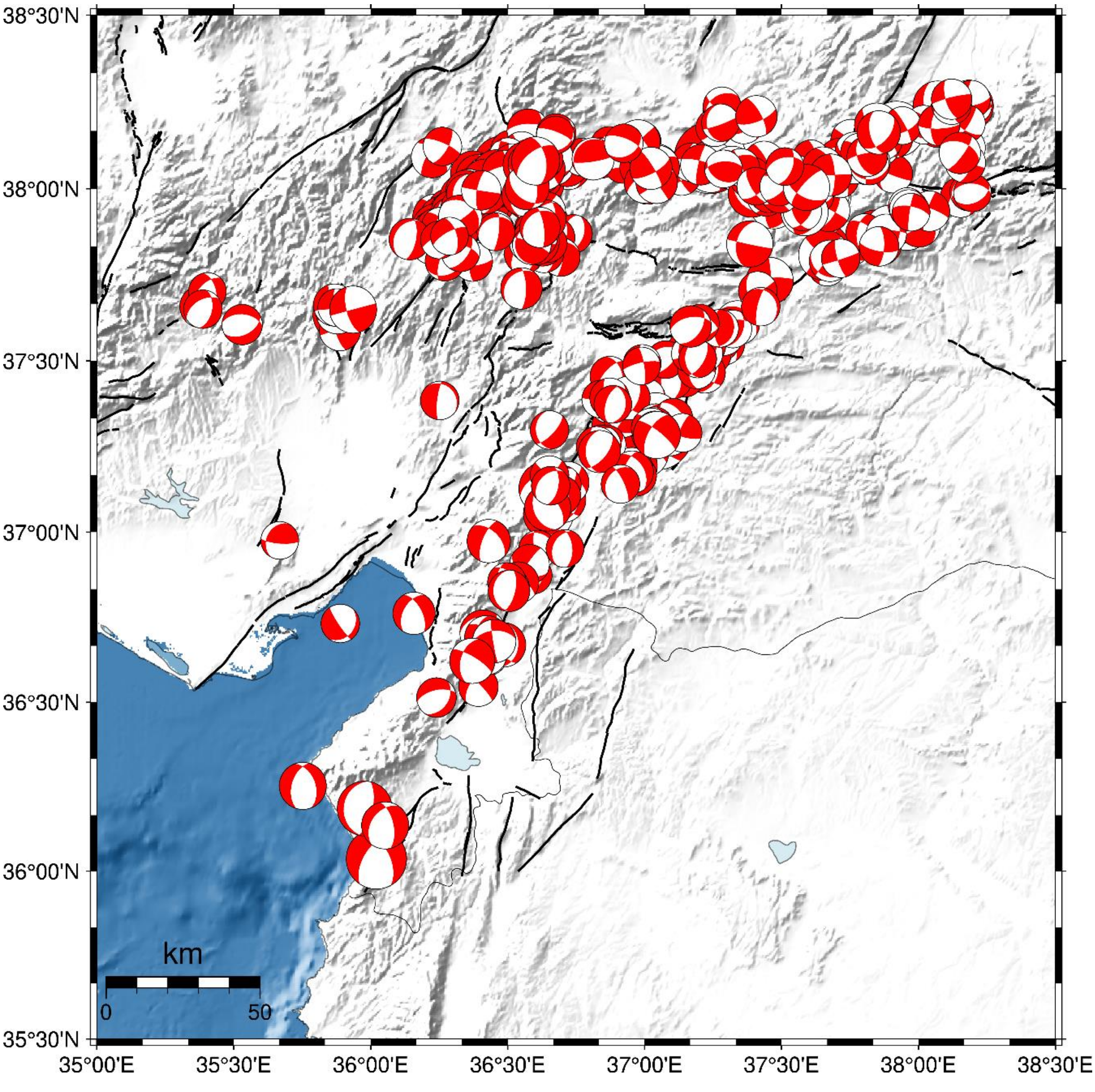

Figure 2.5. Focal mechanism solutions corresponding to the 2023 doublet earthquakes and their aftershocks with magnitude of >4.

3. METHODOLOGY

3.1. Coulomb Stress Change

The Coulomb stress change model has been extensively used to observe the distribution of aftershocks and the triggering of other mainshocks following a major event (Stein et al., 1997; Toda et al., 2011; Durand et al., 2013). During earthquakes, accumulated stress is released, and slip occurring on a fault causes deformation and changes in the static stress distribution around the fault plane (Scholz, 2002). The Coulomb Failure Stress change (CFS) is used to examine how stress from the source fault alters the failure potential on the receiver fault. A source fault where the earthquake occurs, and a receiver fault is defined as a nearby fault that is affected by the stress change. The following formula represents the Coulomb stress change:

$$\Delta \mathrm{CFS} = \Delta\tau + \mu' \Delta\sigma_{\mathrm{n}} \quad (3.1)$$

In the equation (3.1), $\Delta\tau$ represents the change in shear stress in the positive direction of slip, σ_{n} indicates the change in normal stress which is positive for unclamping or confining, and μ' is the effective coefficient of friction, accounting for pore pressure changes and the material properties of the fault zone (King et al., 1994). Positive changes in ΔCFS indicates increased stress, whereas negative changes in ΔCFS represent the stress shadows after an earthquake (Harris, 1998).

Accurate determination of key parameters plays a crucial role in calculating coulomb stress analysis and eliminating uncertainties in coulomb stress change model. These parameters include the location of the earthquake, strike, rake, and dip angles, depth, magnitude as well as physical parameters: Young module, coefficient of friction and Poisson’s ratio.

3.2. B-value Analysis

The frequency-magnitude distribution (FMD) of earthquakes during a specified time period and a given region can be expressed by Gutenberg-Richter Law (Gutenberg and Richter, 1944), which is widely used in seismology to investigate seismicity of the regions. This empirical power-law relation can be expressed as:

$$\text{Log } N(M) = a - bM \tag{3.2}$$

In the equation (3.2), N denotes the cumulative number of earthquakes with a magnitude equal to or exceeding M. ‘a’ and ‘b’ are constants, which are known as seismicity parameters of Gutenberg-Richter relation. The parameter a, referred to as the a-value, represents the earthquake activity rate of a region and it relies on some factors such as the length of the observation period, the size of the considered area. The parameter b, known as the b-value, corresponds to the slope of the FMD chart, and it defines the frequency of minor earthquakes in a region in comparison to major ones. Among these parameters, the b-value has received the great attention in seismicity studies due to its importance in earthquake hazard assessment.

The b-value is not only the parameter used to determine the slope of FMD plots by using the empirical information of the relative proportion of small and large earthquakes in an area, it also shows the tectonic characteristics in a given region (Wyss, 1973). It typically varies between 0.3 and 2.5; when its value is around 1, it is interpreted that the considered area is seismically stable (Frohlich and Davis, 1993). There are several reasons that can cause the spatial variations and temporal changes in determining the b-value. Some of these significant factors are described below:

(i) The crustal structure: an increased heterogeneity due to rock deformations (faulting, fracturing, and cracking), fluid and high pore pressure, liquid and magmatic intrusions may increase the b-value (Mogi, 1962; Ogata et al., 1991; Lin et al., 2007).

(ii) Stress and strain conditions: Tectonic stress is inversely proportional to b-values (Mogi, 1967; Scholz, 1968).

(iii) Volcanic activity: The presence of magma chambers often correlates with high b-values in volcanic regions (Murru et al., 1999; Lin et al., 2007).

(iv) Tectonic settings and focal mechanism: Reverse faults have b <1, strike-slip faults around b ~1, and normal faults b >1 (Amelung and King, 1997; Schorlemmer et al., 2004).

(v) Decreased b-values over timescales of a few years or more are linked to the occurrence of a major earthquakes. The fluctuations in temporal variations show different stages of the earthquake cycle, including stress-buildup, coseismic rupture and aftershocks (Scholz, 1968; Wyss and Lee, 1973; Wiemer and Wyss, 2000).

Therefore, it can be concluded that low b-values may result in high strain rate, high level of accumulated stress, and less heterogeneity. Temporal and spatial variations of the b-value can be considered as an important precursor for determining regions which may precede major earthquakes.

Before calculating the b-value, applying a seismicity declustering method is a mandatory step in seismology studies. Earthquake catalogs typically include foreshocks, mainshocks, and aftershocks. Declustering is a process that separates dependent events, such as aftershocks, from independent events like mainshocks, to achieve a catalog of background seismicity. The goal of isolating seismicity is to enable more accurate statistical analysis (Stiphout et al., 2012). There are several methods for declustering process. The methods proposed by Gardner and Knopoff (1974), as well as Reasenberg (1985), have been widely used by the majority of users because they are easily accessible and simple to utilize with ZMAP Software. The Reasenberg declustering method was used to obtain background seismicity in this study.

After isolating independent earthquakes, Cumulative Visual Inspection method (CVI) was used to determine the temporal period of completeness in the catalog (Tinti and Mulargia, 1985). CVI method detects the deviation point in the cumulative number of earthquakes against time. In the EAFZ, various researchers, including Öztürk (2018), Ali and Akkoyunlu (2022), Polat (2022), Alkan et al. (2023) have applied this method in order to enhance b-value analysis by identifying the initial year that marks the beginning of the analysis period. To determine Magnitude of completeness (Mc) values, the maximum curvature (MAXC) method was used. The FMD curve's maximum value for the first derivative is used to define the point of maximum curvature. In other words, it defines the slope of the FMD chart. The code of this method is freely available in ZMAP software.

There are numerous approaches to determine the b-value. The Maximum-Likelihood (ML) and the Least-squares regression methods are the most frequently used for estimating the b-value. Among these two approaches, the ML method is world-widely more utilized and more accepted for estimating reliable b-values. Because of its efficiency and robustness, the ML method was used to calculate the b-values in the study area. It was originally proposed by Aki (1965) and then revisions were made by Utsu (1965). The formula for this approach can be written as follows:

$$b = \frac{\log_{10}(e)}{\overline{M} - (Mc - \frac{\Delta M}{2})} \qquad (3.3)$$

In the equation (3.3), where $\overline{M}$ is the mean magnitude, ΔM is the magnitude interval and the magnitude of completeness is the Mc.

3.3. Magnitude of Completeness

Magnitude of completeness (Mc) is expressed as the minimum earthquake magnitude that can be reliably detected by seismograph networks within a given spatial and temporal domain (Rydelek and Sacks, 1989). Since earthquake catalogs are product of networks, Mc physically depends on the detection capability of any seismic networks. For instance, a network's ability of detection is affected by several factors including site condition, station distribution, density of seismic stations and data processing steps. When there is an error in the network, it propagates into earthquake catalogs. These errors affect the estimation of the Mc, and to compute incorrect Mc values lead to errors in seismic parameters. Evaluating Mc in instrumental earthquake catalogs is a crucial step for seismicity analysis. In fact, if Mc is underestimated, b-value will also be underestimated. On the other hand, overestimating Mc values leads to a loss of information and results in larger standard deviations (Ogata and Katsura, 1993; Mignan and Woessner, 2012).

Theoretically Mc is not a fixed value. Mc is assessed by two distinguished methods: Catalog-based and Network-based method (Mignan and Woessner, 2012). Catalog-based approaches are the Maximum Curvature Technique (Wiemer and Wyss, 2000), the Goodness of fit test (Wiemer and Wyss, 2000), the Mc by b-value stability approach (Cao and Gao, 2002), the entire magnitude range methods (Woessner and Wiemer, 2005), the Median-based analysis of the segment slope (Amorèse, 2007) and the day-to-night noise modulation (Rydelek and Sacks, 1989). Network based methods are wave forward simulation (D'Alessandro et al., 2011) and probabilistic magnitude of completeness (Schorlemmer and Woessner, 2008). As I mentioned above, the MAXC method was used to define Mc.

3.4. Interferometric Synthetic Aperture Radar Technique

Interferometric Synthetic Aperture Radar (InSAR) is a remote sensing technique that enables the detection of Earth's surface deformations and topographic features through the use of radar signals with centimeter- to millimeter-level accuracy. The fundamental theoretical basis of InSAR lies in the exploitation of the phase difference between two or more SAR (Synthetic Aperture Radar) images obtained from slightly different spatial or temporal perspectives.

Each SAR image is composed of complex pixels containing amplitude and phase information. The phase of the radar signal is directly related to the distance between the satellite sensor and the target on the Earth's surface. When two SAR acquisitions, known as the master and slave images, of the same region are compared, their phase difference can be used to produce an interferogram. The interferometric phase can be expressed as (Massonnet and Feigl, 1998; Hanssen, 2001):

$$\varphi_{\mathrm{int}} = \varphi_{\mathrm{topo}} + \varphi_{\mathrm{def}} + \varphi_{\mathrm{atm}} + \varphi_{\mathrm{orb}} + \varphi_{\mathrm{noise}} \tag{3.4}$$

In the equation (3.4), φ_{topo} represents the phase component due to topographic height differences, φ_{def} represents the phase caused by ground deformation, φ_{atm} accounts for atmospheric phase delays, φ_{orb} indicates the orbit inaccuracies, φ_{noise} represents the temporal or spatial decorelation. To accurately extract ground deformation from the interferometric phase, the unwanted contributions from topography, atmospheric delays, and satellite orbit errors must first be removed. This is typically done by using a digital elevation model (DEM) to eliminate topographic effects, applying filtering techniques to reduce atmospheric noise, and incorporating precise orbit data to correct orbital inaccuracies.

Several Earth observation satellite missions equipped with SAR sensors have been launched in recent decades to monitor surface deformation, land use, and natural hazards. These missions vary in terms of radar frequency, spatial resolution, revisit time, and application focus. The most widely used SAR satellite missions is shown in Table 3.1**.**

Table 3.1. SAR satellite missions.

Satellite Mission	Agency	Radar Band	Revisit Time	Key Applications
Sentinel-1A/B/C	ESA	C-band	6–12 days	Ground deformation, flood mapping, co-seismic studies
ALOS-2 (PALSAR-2)	JAXA	L-band	~14 days	Vegetation, tectonics, landslides, agriculture
TerraSAR-X / TanDEM-X	DLR / Airbus	X-band	~11 days (TanDEM-X)	DEM generation, urban studies, infrastructure monitoring
RADARSAT-2 / RCM	CSA	C-band	Daily (RCM constellation)	Ice monitoring, subsidence, maritime surveillance
SAOCOM 1A/1B	CONAE / ASI	L-band	~16 days	Soil moisture, flood events, earthquake deformation
COSMO-SkyMed (1st and 2nd Gen)	ASI	X-band	Up to daily (constellation)	Subsidence, infrastructure, emergency response

Many remote sensing satellites follow near-polar orbits, and their combination with the Earth's rotation from west to east, allow for global coverage over a specific time interval. During the ascending orbit, the satellite travels from the southern hemisphere toward the North Pole whereas, in the descending orbit**,** it moves from the northern hemisphere toward the South Pole. This orbital configuration enables repeated observations of the same area from different viewing geometries, which is essential for interferometric applications.

InSAR technology is widely applied in the study of both tectonic and non-tectonic surface processes. It is commonly used to monitor earthquakes, volcanic activity, slow-moving landslides, glacier flow, groundwater level variations, and subsidence related to fluid extraction or drilling activities. InSAR technique enables the detection, measurement, and monitoring of crustal changes associated with various geophysical processes. Among its many geophysical and environmental applications, it is particularly valuable for studying co-seismic deformation which refers to ground displacement that occurs during an earthquake. By generating interferograms from pre- and post-event SAR acquisitions, it becomes possible to detect and map surface ruptures, quantify slip distribution, and analyze displacement patterns across large regions. These observations are critical for enhancing seismic hazard assessments and improving our understanding of fault dynamics. InSAR technique was used in this study to understand the deformation in the study region caused by the 2023 Kahramanmaraş earthquakes.

4. ANALYSIS AND RESULTS

4.1. Coulomb Stress Change Analysis

First of all, earthquakes in the study area were selected from the mainshock (Mw 7.7) to the second shock (Mw 7.6) and static stress transfer between these two events, which appear to be temporally and spatially related, was evaluated to better understand whether the mainshock triggered the second shock or not. Subsequently, to assess the current stress distribution in the region, a combined Coulomb Stress Change analysis was performed using 47 earthquakes with magnitudes equal to or exceeding Mw 5.0 that occurred between 2023 and the end of 2024 (Table 4.1).

Focal mechanism data obtained from the AFAD is given in Table 4.1 showing strike, dip and rake (S/D/R) values for the first and second nodal planes. Coulomb 3.4 software (Lin and Stein, 2004) was used to calculate Coulomb stress variation in the study area. Due to the continental strike-slip faulting mechanism, the coefficient of friction was selected as 0.4 based on the elastic dislocation modelling (Parsons et al., 1999). In an elastic half-space framework, earthquake ruptures are modeled as rectangular dislocations, with a Young’s modulus of 80 GPa and Poisson’s ratio of 0.25 (Okada, 1992; Toda et al., 2005)

Table 4.1. List of focal mechanism solutions.

Date	Latitude	Longitude	Magnitude	Depth	S/D/R	S/D/R
2023-02-06 01:17:32	37,288	37,043	7,7	8,6	233/74/18	140/77/168
2023-02-06 01:26:49	37,235	36,992	5,6	6,98	294/68/-170	200/81/-22
2023-02-06 01:28:16	37,304	36,92	6,6	6,2	300/70/-128	187/43/-30
2023-02-06 01:36:28	37,128	36,639	5,7	11,19	26/56/-121	254/45/-52
2023-02-06 01:51:44	37,542	37,188	5,3	6,63	125/37/-79	292/53/-98

Table 4.1. List of focal mechanism solutions. (cont.)

Date	Latitude	Longitude	Magnitude	Depth	S/D/R	S/D/R
2023-02-06 01:58:23	37,054	36,649	5,3	10,21	29/28/24	278/79/115
2023-02-06 02:01:44	37,294	37,006	5,3	16,44	358/32/-71	156/60/-101
2023-02-06 02:03:35	37,898	37,957	5,6	10,23	241/56/31	133/65/142
2023-02-06 02:23:13	37,194	36,955	5,3	11,81	168/39/-163	64/79/-52
2023-02-06 06:54:57	37,733	37,457	5	7	357/85/-170	266/80/-6
2023-02-06 10:24:47	38,089	37,239	7,6	7	358/73/174	90/86/13
2023-02-06 10:32:08	38,064	37,241	5,5	10,93	75/78/23	340/68/167
2023-02-06 10:35:57	38,172	37,92	5,9	11,28	31/31/32	273/74/117
2023-02-06 12:02:11	38,071	36,478	5,9	17,04	9/56/-95	198/35/-82
2023-02-06 12:13:45	37,988	37,483	5,1	7	118/84/60	18/30/168
2023-02-06 13:17:42	38,0897	36,59	5,2	10,85	11/42/-93	195/49/-87
2023-02-06 13:39:23	38,037	37,628	5,3	7,2	316/87/145	48/55/4
2023-02-06 13:44:49	38,007	37,555	5,1	8,76	271/22/-50	49/73/-105
2023-02-06 15:14:32	37,977	37,667	5	7,04	30/74/170	123/80/16
2023-02-06 15:33:31	38,239	38,182	5,3	11,15	244/70/13	150/78/160
2023-02-06 16:43:27	38,024	36,472	5,1	10,06	360/67/-135	249/50/-31
2023-02-06 18:03:54	38,043	36,484	5,2	12,79	355/66/-148	251/61/-28
2023-02-06 18:05:01	38,004	36,403	5	7,03	47/57/-91	228/33/-89
2023-02-06 20:37:51	37,293	37,046	5,5	5,96	171/49/-74	327/43/-108
2023-02-06 20:40:05	38,24	38,07	5,2	5,82	162/45/-172	66/84/-45
2023-02-06 21:15:17	38,062	37,04	5	17,4	68/72/3	337/87/162
2023-02-07 03:08:55	37,975	37,629	5	6,87	8/69/142	114/55/26

Table 4.1. List of focal mechanism solutions. (cont.)

Date	Latitude	Longitude	Magnitude	Depth	S/D/R	S/D/R
2023-02-07 03:13:12	37,808	37,655	5,4	8,44	224/83/-173	133/83/-7
2023-02-07 15:48:52	37,959	36,434	5,2	11,48	197/34/-111	42/59/-77
2023-02-07 18:09:58	38,085	36,62	5	10,22	295/70/-146	192/59/-24
2023-02-07 21:21:25	37,952	37,471	5	15,84	189/62/89	10/28/91
2023-02-08 07:48:31	38,021	36,467	5,1	9,06	245/61/-45	1/52/-142
2023-02-08 11:11:51	38,012	37,641	5,3	13,18	300/62/20	200/72/150
2023-02-08 14:20:25	37,985	37,391	5	16,69	135/40/-77	299/51/-100
2023-02-10 04:50:23	38,235	38,141	5	10,45	247/81/1	156/89/171
2023-02-16 19:47:50	36,253	35,752	5,1	9,26	339/45/-118	196/51/-65
2023-02-18 19:31:31	38,08	36,602	5,1	6,2	349/54/-138	231/57/-45
2023-02-20 17:04:27	36,037	36,021	6,4	21,73	214/57/-44	332/55/-138
2023-02-20 17:07:34	36,186	35,978	5,8	6,64	13/66/-88	187/24/-95
2023-02-23 15:53:47	36,136	36,053	5	8,75	216/40/-49	347/61/-119
2023-02-27 02:51:20	37,932	37,584	5	8,51	203/53/95	14/37/83
2023-03-03 02:53:42	37,847	36,602	5	7,06	22/45/-91	204/45/-89
2023-03-23 09:19:51	38,04	36,459	5,3	12,9	357/46/-153	248/71/-47
2023-05-03 17:16:38	38,069	36,569	5	7	32/39/-79	199/52/-99
2023-07-25 05:44:49	37,634	35,884	5,5	10,38	232/68/-15	327/76/-158
2024-09-07 06:31:10	37,2842	37,0447	5	7	210/60/-16	308/76/-149
2024-10-27 17:07:09	37,6497	35,9358	5	9,7	75/90/-23	166/67/-180

Coulomb stress change analysis was initially performed after the first mainshock at 5 km and 10 km depths (Figure 4.1) (Figure 4.2). The dataset includes the mainshock and the subsequent nine aftershocks with magnitudes equal to or greater than Mw 5.0, all occurring before the second shock. This analysis shows that in the northeast direction, stress increased in Adıyaman and Malatya, while in the northwest, it increased in the Göksun-Elbistan region. In the Gulf of Iskenderun, and further south in Hatay, stress also increased especially at shallow seismogenic depths of 5 km. Along the fault zone and in all four mentioned directions, high stress values (+0.1 bar) and positive stress changes were observed within the region of interest. In contrast, negative stress values (-0.1 bar) were observed in Gaziantep and Şanlıurfa in the southeast, as well as in Adana, Osmaniye and the northern part of Kahramanmaraş in the southwest.

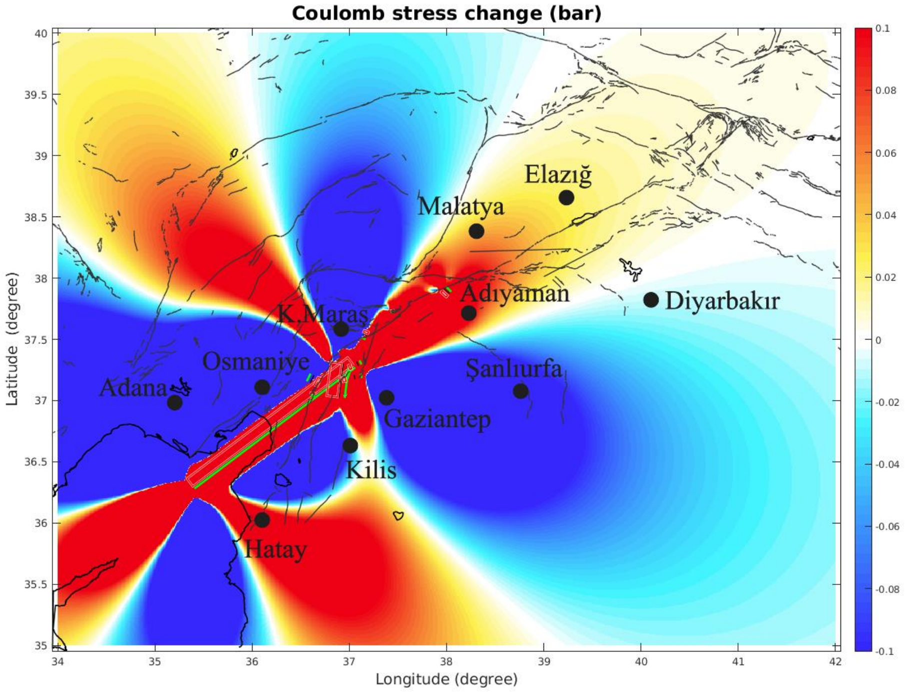

Figure 4.1. Coulomb stress changes resulting from the first shock (Mw 7.7) and the subsequent nine aftershocks (Mw ≥ 5) evaluated up to second shock in the region at a depth of 5 km.

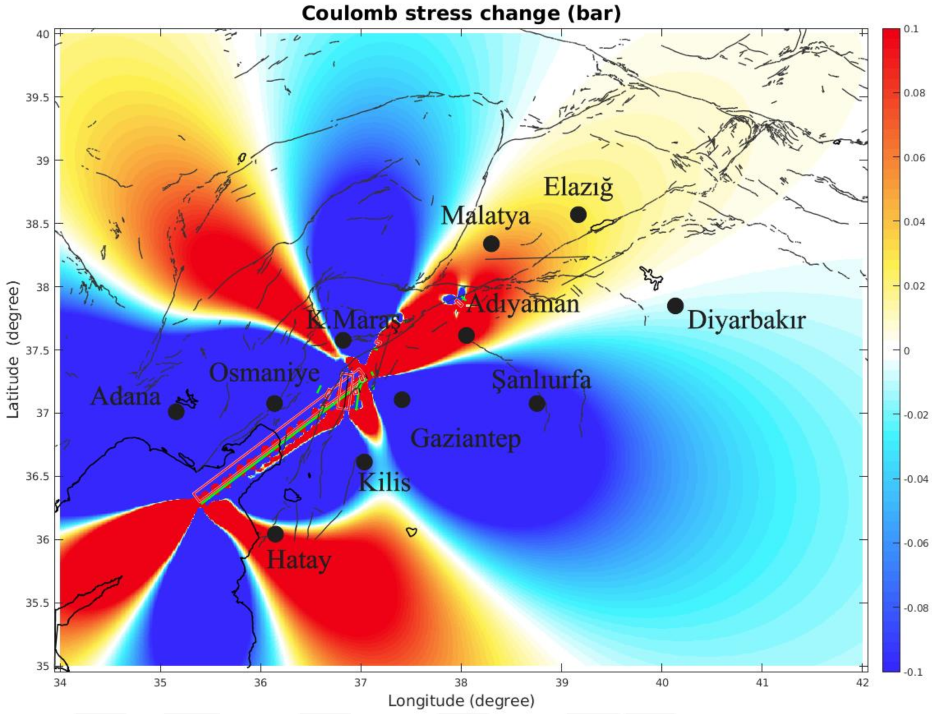

Figure 4.2. Coulomb stress changes resulting from the first shock (Mw 7.7) and the subsequent nine aftershocks (Mw ≥ 5) evaluated up to second shock in the region at a depth of 10 km.

The second coulomb stress change analysis was performed for events with magnitudes equal to or larger than Mw 5.0, from the second shock to the end of 2024 at a depth of 5 km and 10 km (Figure 4.3) (Figure 4.4). Positive stress changes were observed in Diyarbakır to the east, and in the south in Gaziantep and Kilis. In the west, around Göksun, and toward the north between Malatya and Elazığ, stress increases were also observed at depths of 0-10 km.

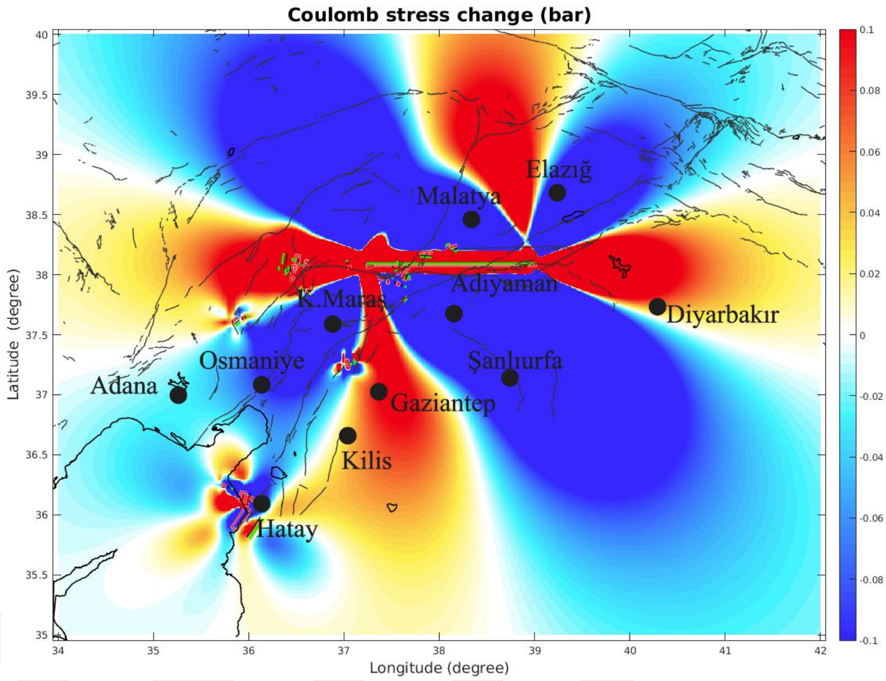

Figure 4.3. Coulomb stress changes resulting from the second shock (Mw 7.6) and the subsequent aftershocks examined in the region at a depth of 5 km.

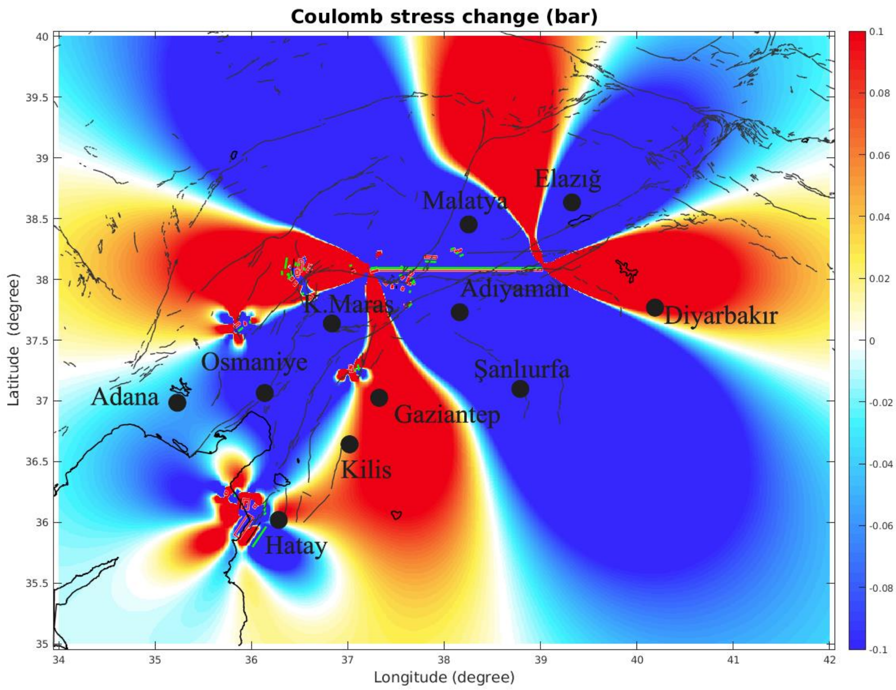

Figure 4.4. Coulomb stress changes resulting from the second shock (Mw 7.6) and the subsequent aftershocks examined in the region at a depth of 10 km.

The final coulomb analysis was performed for all earthquakes that occurred in the study region with magnitudes equal to or greater than 5.0 Mw between 2023 and 2024, at depths of 5 km and 10 km (Figure 4.5) (Figure 4.6). According to the results, high stress values were observed at shallow crustal depths in several regions: the Gulf of İskenderun near the Karataş and Yumurtalık faults, and the area near the Düziçi-İskenderun fault extending toward the Cyprus Arc in the southwest; in the northeast, along the Malatya-Elazığ toward the Pütürge segment and Karlıova triple junction direction; around the Göksun bend and the Savrun Fault in the west; along the Hatay-Syria border; and between Kilis and the city of Gaziantep in southeast.

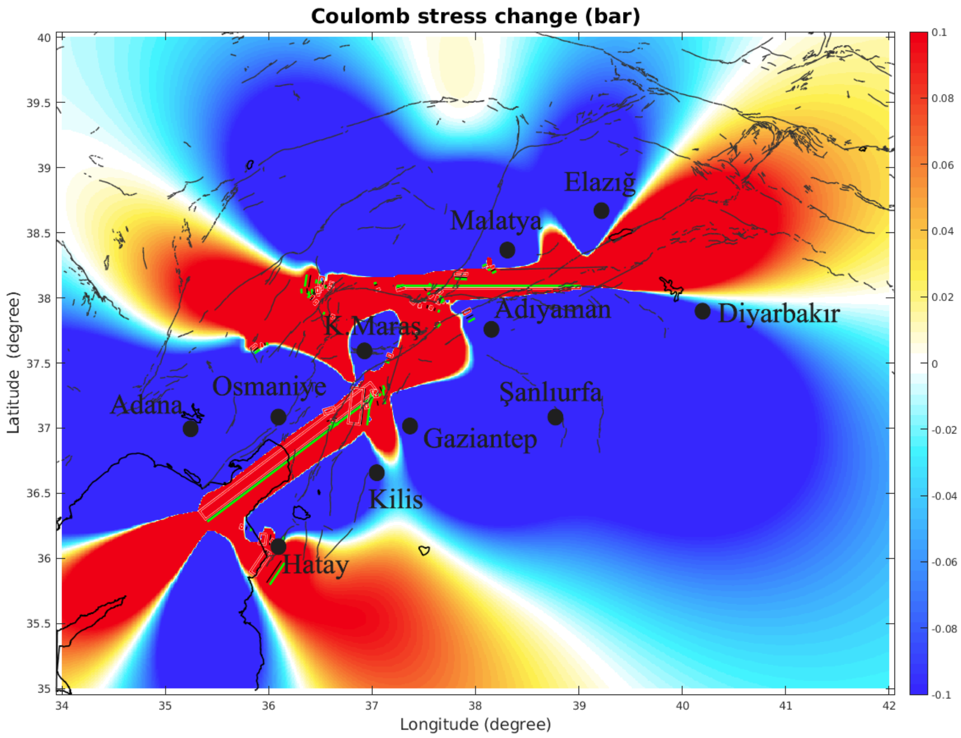

Figure 4.5. Coulomb stress change model at 5 km depth, occurring after mainshock and continuing through the end of 2024.

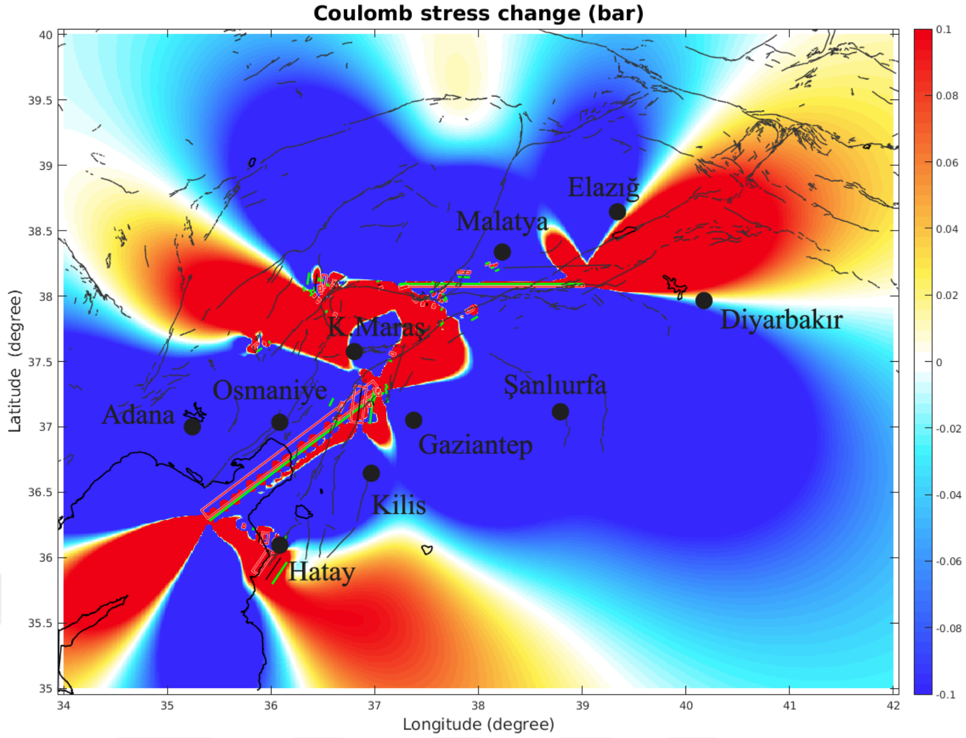

Figure 4.6. Coulomb stress change model at 10 km depth, occurring after mainshock and continuing through the end of 2024.

To illustrate the direction of strike of the earthquakes, coulomb stress changes were also calculated separately for the mainshock at 8.6 km depth (Figure 4.7), with horizontal displacement vectors illustrated in Figure 4.8, and for the second shock at a depth of 7 km (Figure 4.9), with horizontal displacement vectors shown in Figure 4.10. The areas with the greatest density and length of vectors generally indicate the areas experiencing the most deformation. These areas are where aftershocks are likely to intensify and ruptures may propagate.

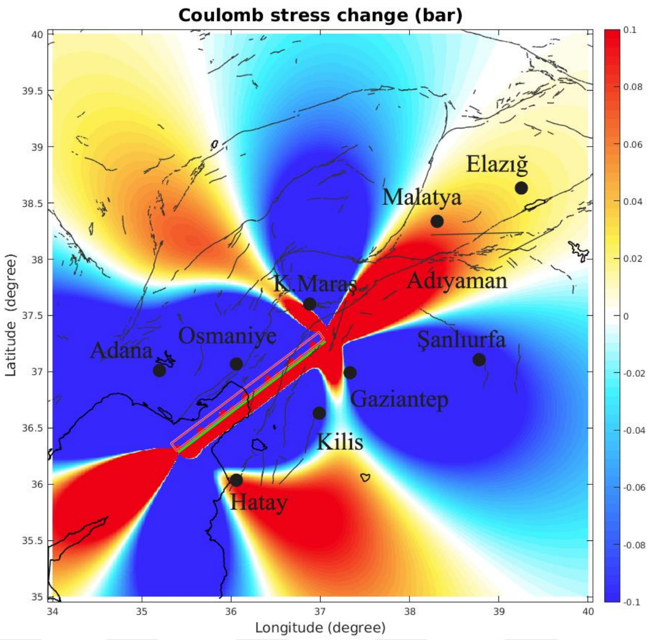

Figure 4.7. Coulomb stress change model of the mainshock (Mw 7.7) at a depth of 8.6 km. The catalog information was taken from AFAD. Active faults are illustrated in black lines (Emre et al., 2013).

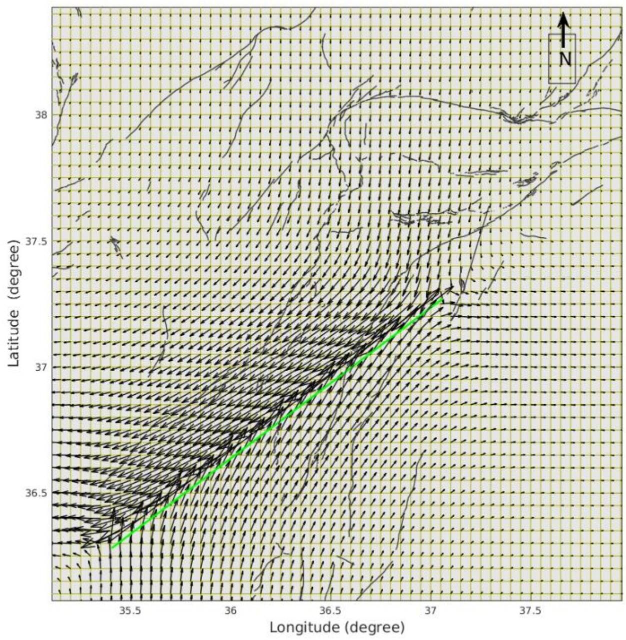

Figure 4.8. The horizontal displacement vectors of the Mainshock (Mw 7.7). The Dataset was taken from AFAD and the black lines show the active fault line (Emre et al., 2013).

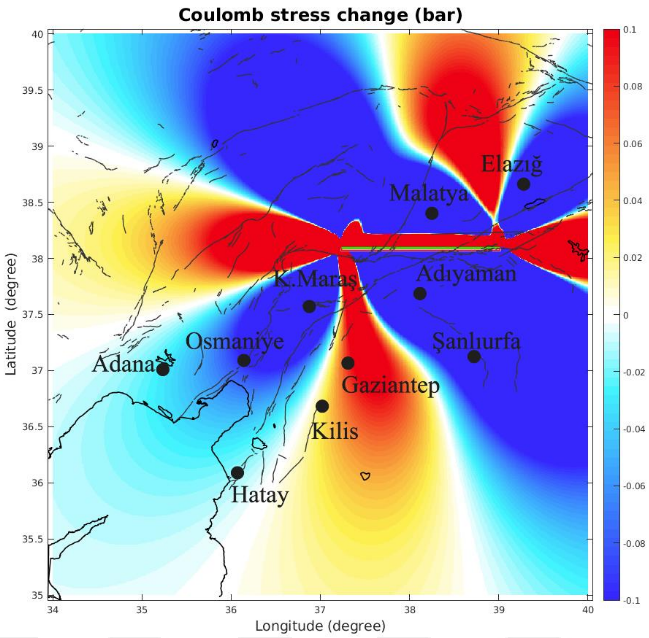

Figure 4.9. Coulomb stress change of the second shock (Mw 7.6) at a depth of 7 km. The catalog information was taken from AFAD. Active faults are illustrated in black lines (Emre et al., 2013).

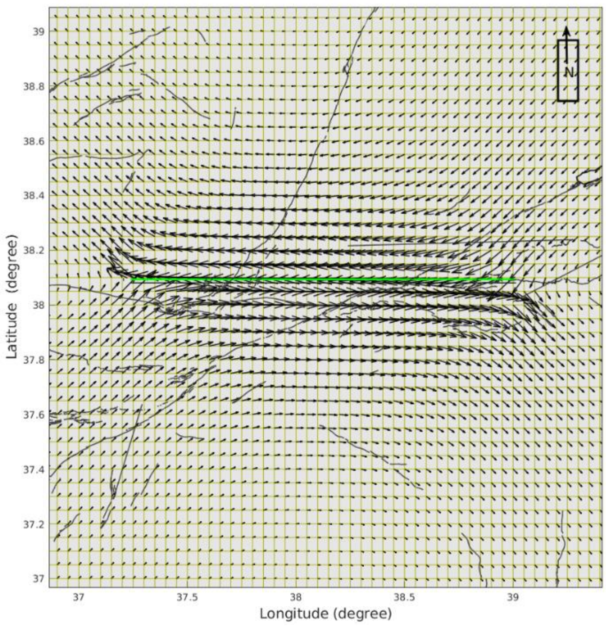

Figure 4.10. The horizontal displacement vectors of the second shock (Mw 7.6). The Dataset was taken from AFAD and the black lines represent the active fault line (Emre et al., 2013).

In addition to Coulomb Stress Change analysis, the mainshock, the second shock and their aftershocks from 2023 to 2024 were plotted on a topographic map to compare the results with the coulomb stress analysis (Figure 4.11).

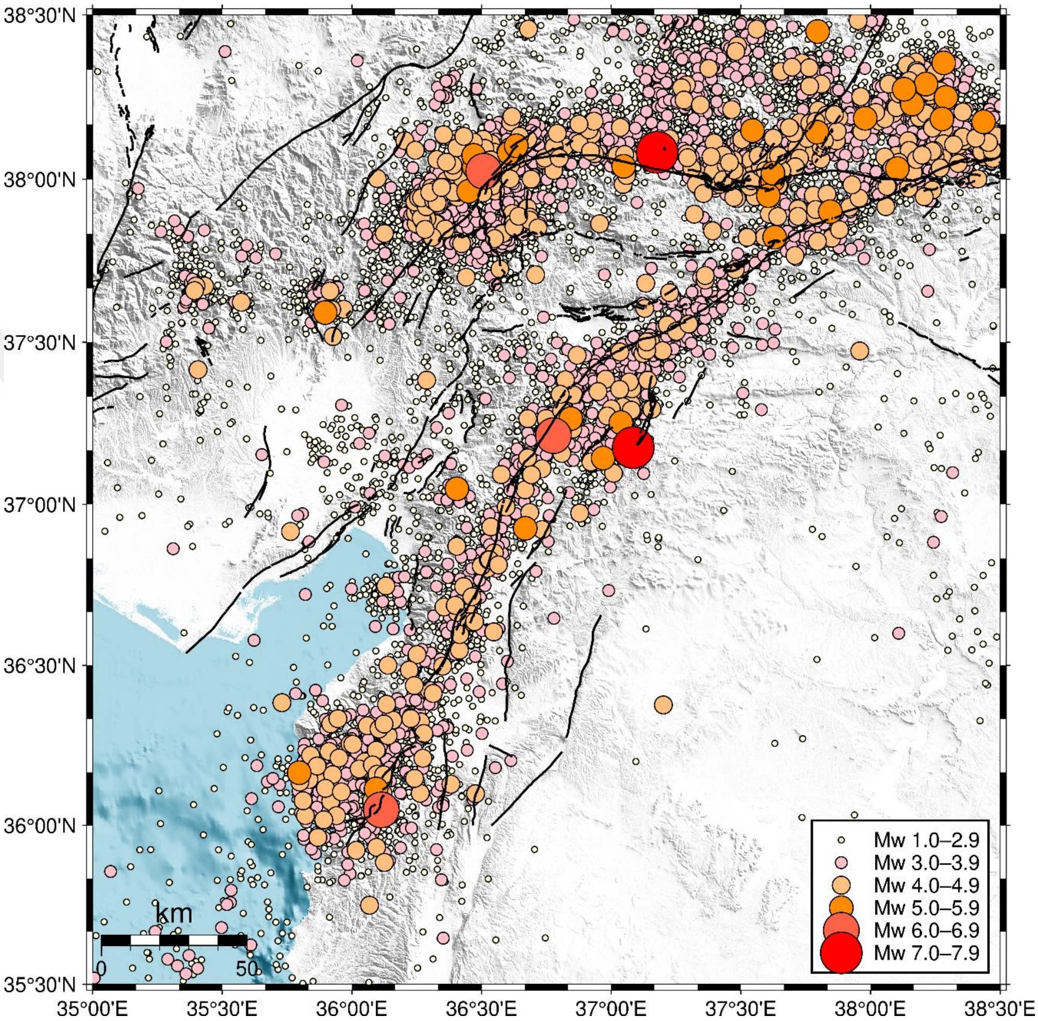

Figure 4.11. The 2023 doublet earthquakes and their aftershocks for the time period between 2023 and 2024. The Dataset was taken from KOERI.

4.2. The Spatial and Temporal Analysis of b-Value

The data utilized in this study were obtained from the KOERI, covering the period from the beginning of 1900 to the end of 2024. The b-value analysis was performed within the region bounded by 34.5°-38.5°E and 35.5°-38.5°N. This dataset includes 29,401 events with magnitudes ranging from 2.0 to 7.8 within the study area. The magnitude conversions from Tan (2021) were used to obtain a homogeneous catalog. All magnitudes were converted to moment magnitude (Mw). To determine the temporal and spatial variations of b-value of the study region, ZMAP Software Package were used. It integrates with MATLAB and comes with a graphical user interface (GUI), that makes easier for users to perform statistical analyses, and visualization of seismicity across space and time (Wiemer, 2001).

In addition to coulomb analysis, spatial and temporal analyses of the b-value were performed for the following time periods: 1995-2004, 2005-2014, 2015-2023, 2023-2024. These intervals were selected to facilitate comparison and to better understand the background seismicity of the study area before and after the doublet earthquakes that occurred in 2023.

Between 1995 and 2004, totally 974 events occurred in the region, with magnitudes in the range of 2.0 to 7.0 (Figure 4.12). The 1998 Adana Earthquake, which had a magnitude of 6.3 Mw, was the largest event. With a fault plane solution of strike=50°, dip=85°, and rake=10°, the mainshock exhibited left-lateral strike-slip mechanism (Aktar et al., 2000).

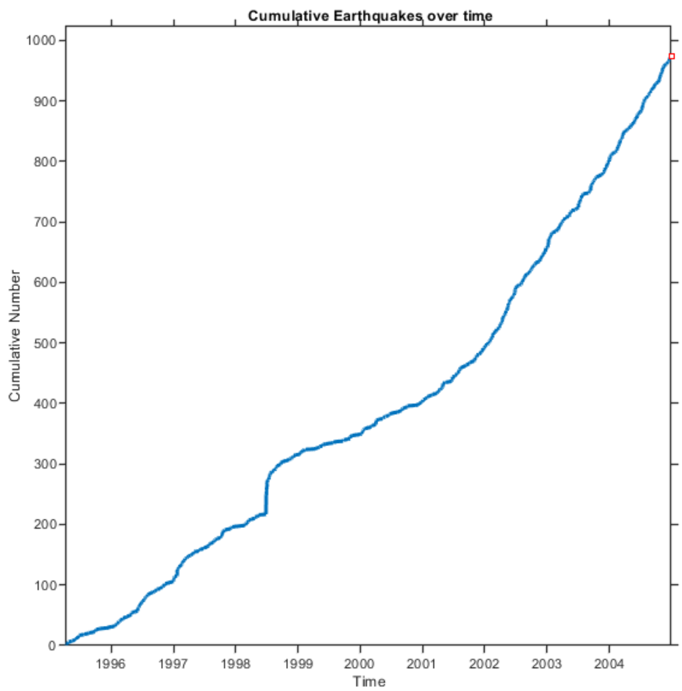

Figure 4.12. Total number of earthquakes recorded from 1995 to 2004.

A total of 916 events were used to calculate spatial variations of b-values across the region. In the spatial analysis, b-values ranged from 0.8 to 1.6. Low b-values were observed around 36.8°-37.2°N-35.5°-36°E, while relatively high b-values were found toward the east and the northeast direction. In this region, Mc was calculated as 3.0 and the average b-value was calculated as 0.93±0.05 (Figure 4.13) (Figure 4.14).

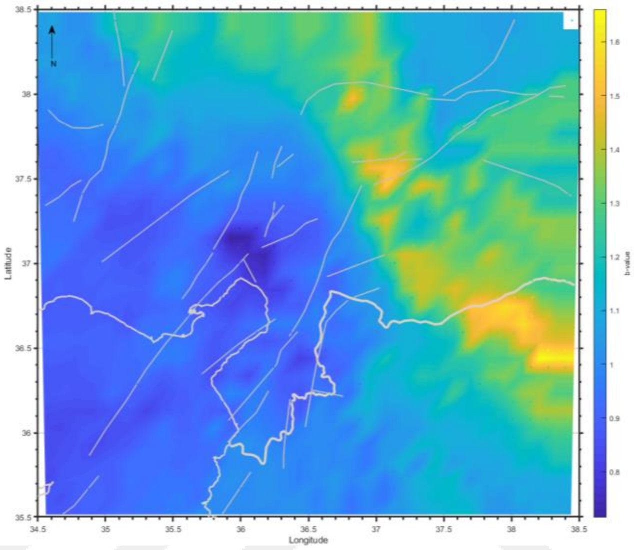

Figure 4.13. The spatial variations of b-value between 1995 and 2004.

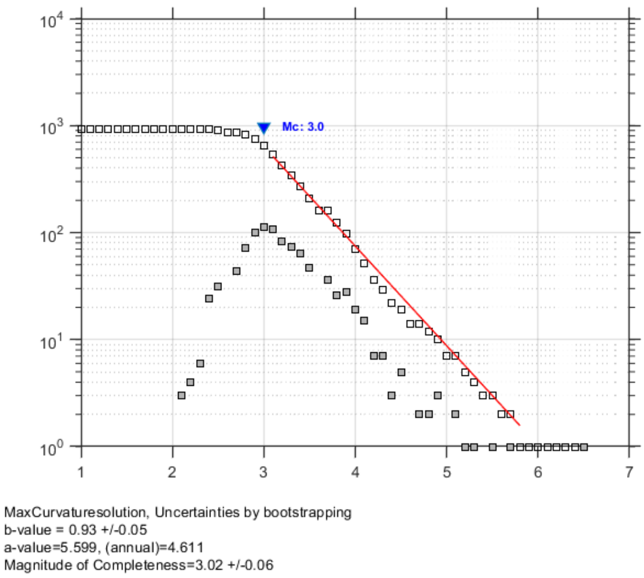

Figure 4.14. FMD chart for the time period between 1995 and 2004.

During the period between 2005 and 2014, a total of 5739 events occurred at depths ranging from 1 to 31 km, covering a magnitude range of Mw 2.0-5.1 (Figure 4.15).

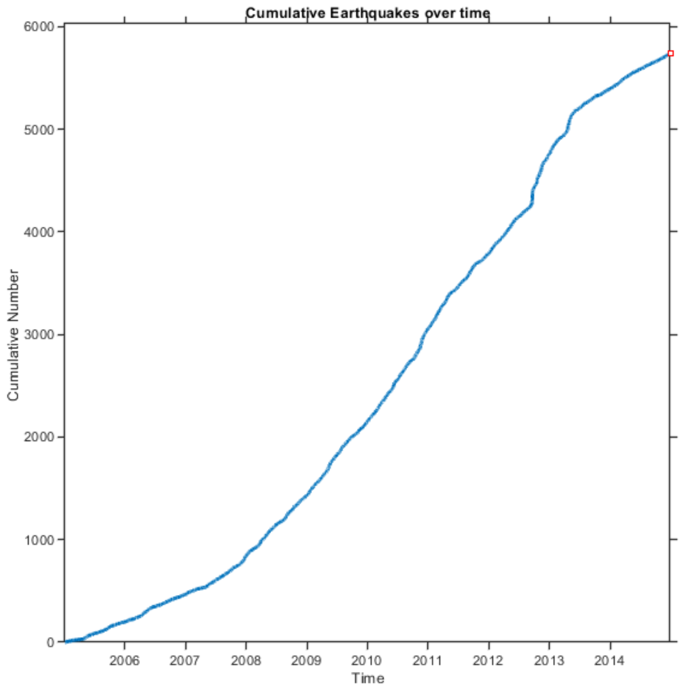

Figure 4.15. Total number of earthquakes recorded from 2005-2014. The Dataset was taken from KOERI.

There were only three events occurring with magnitudes between 5.0 and 5.1. The spatial variation of b-values was ranged from 1.0 to 2.5. The average b-value and Mc were calculated as 1.12±0.04 and 2.5, respectively (Figure 4.16) (Figure 4.17).

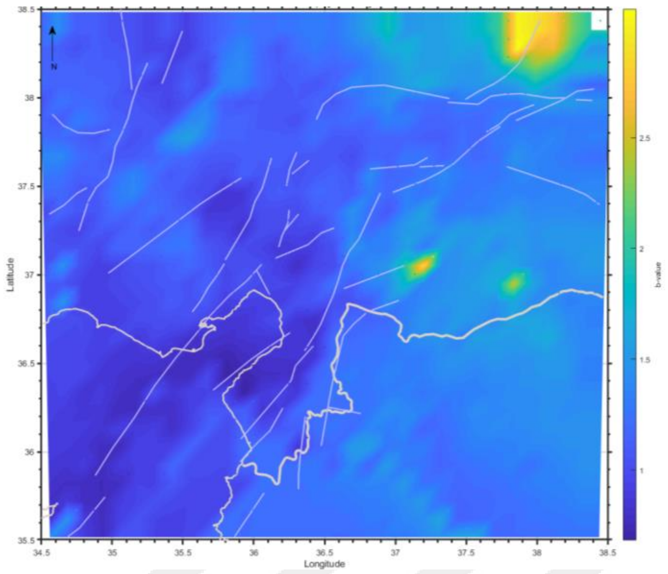

Figure 4.16. The spatial variation of b-value between 2005 and 2014.

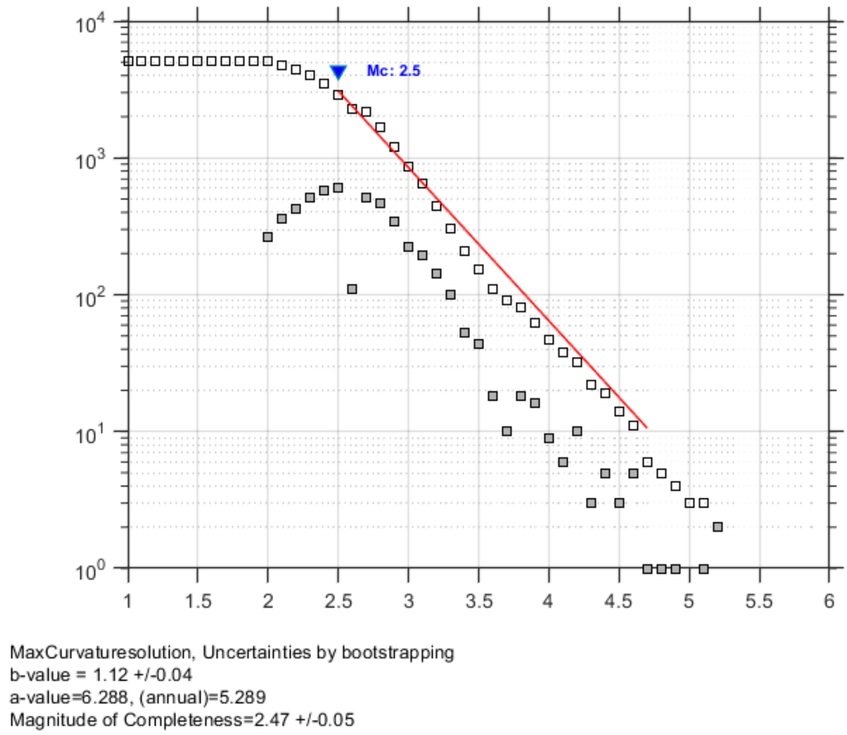

Figure 4.17. The Frequency-magnitude distribution chart for the time period between 2005 and 2014.

Between 2015 and 2023 (up to one day before the 2023 Pazarcık Earthquake), a total of 3008 events occurred at depths between 1 and 31.10 km, with magnitudes ranging from 2.0 to 4.9 Mw (Figure 4.18).

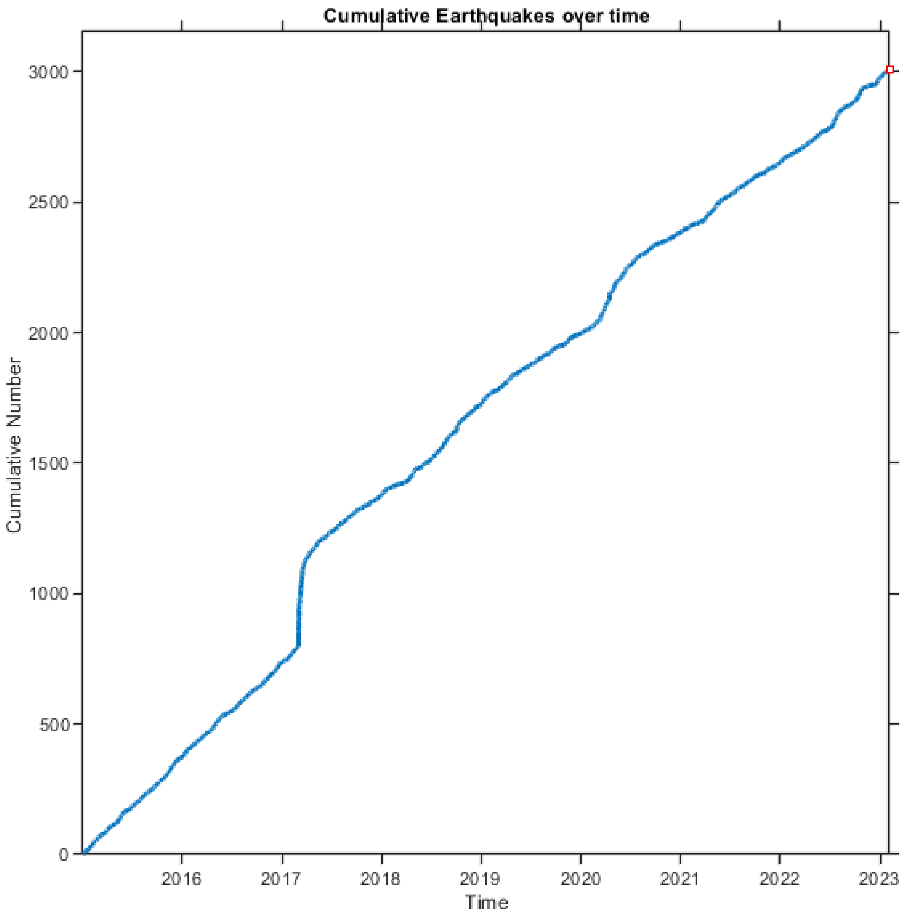

Figure 4.18. Total number of earthquakes recorded from 2015 to 2023. The Dataset was taken from KOERI.

The spatial variation of b-values was calculated using 2425 events, with values ranging from 0.7 to 1.3. In the FMD chart, the average b-value and Mc were calculated as 0.87±0.02 and 2.0, respectively (Figure 4.19 and Figure 4.20).

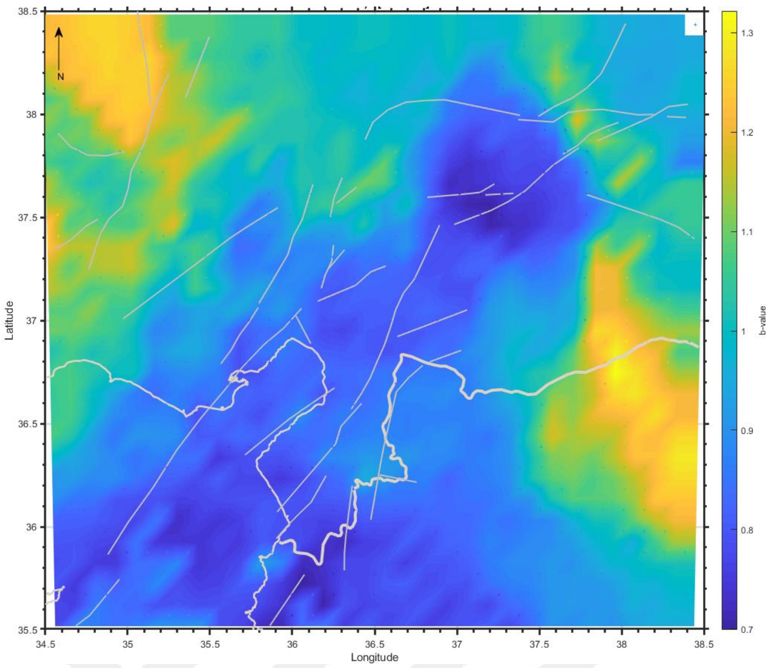

Figure 4.19. The spatial distribution of b-value between 2015 and 2023.

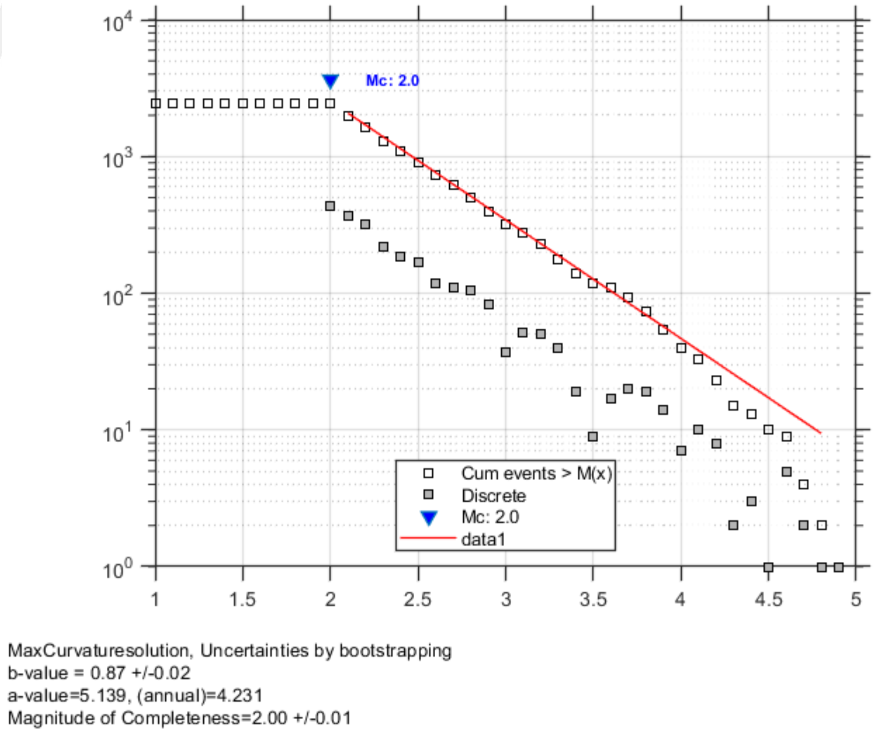

Figure 4.20. The frequency-magnitude distribution chart for the time period between 2015 and 2023.

During the period between 2023 and 2024, the spatial variations in b-values were calculated for the time after the second shock (the 2023 Elbistan Earthquake) up to the end of 2024. A total of 19123 events occurred in the study region, within magnitudes ranging from Mw 2.0 and 7.6 and the depths between 1 km and 39.40 km (Figure 4.21).

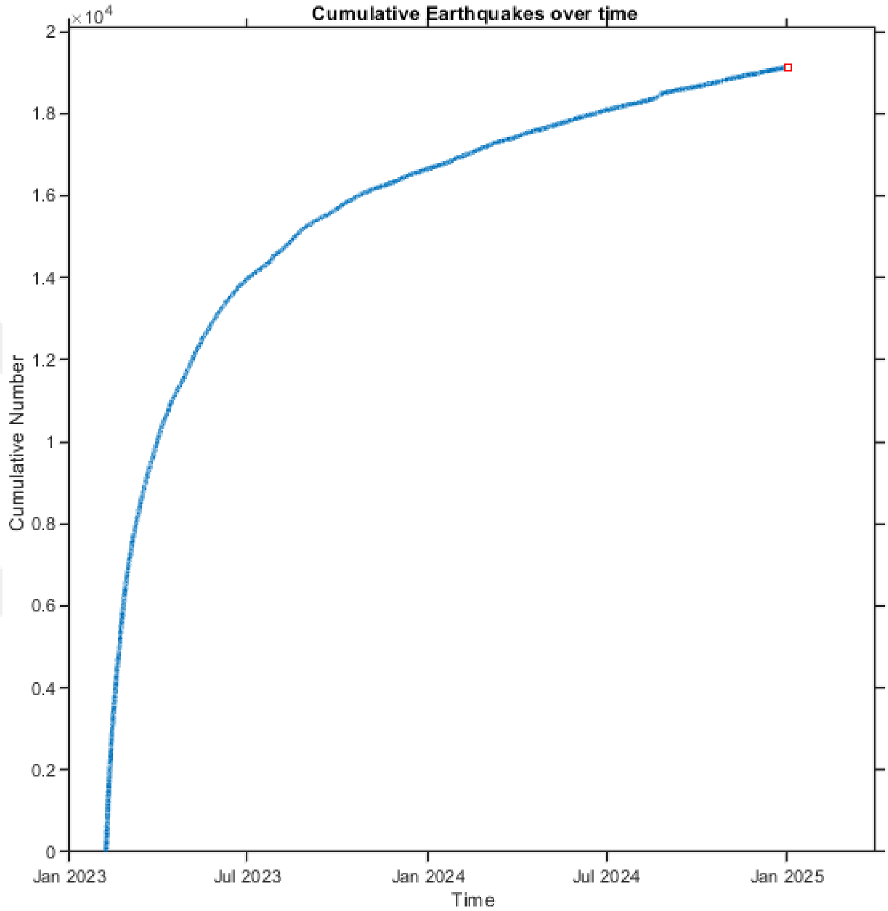

Figure 4.21 Total number of earthquakes between the second shock in 2023 and the end of 2024. The dataset was obtained from KOERI.

The spatial variations of b-values ranged between 0.7 and 1.4, based on 9605 events. The avarage b-value and Mc were calculated as 0.93 and 2.0, respectively. Low b-values were primarily observed in the southern and southwestern regions, particularly between Osmaniye and Gaziantep near the Düziçi-İskenderun fault zone, as well as in Hatay and toward the Cyprus Arc. (Figure 4.22) (Figure 4.23).

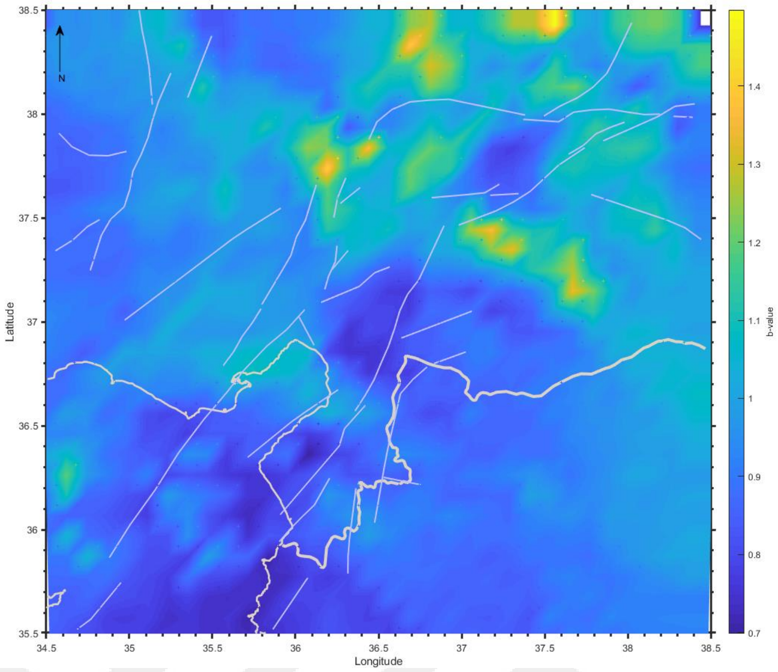

Figure 4.22. The spatial variation of b-value between the second shock in 2023 and the end of 2024.

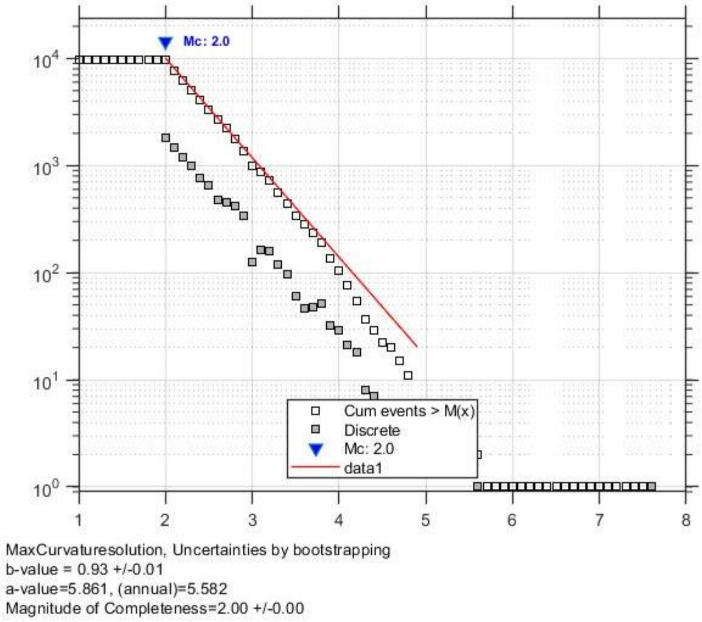

Figure 4.23. The frequency-magnitude distribution chart from the second shock in 2023 to the end of 2024.

A total of 29109 events occurred in the region between 1995 and 2024, ranging in magnitudes from Mw 2.0 up to 7.8 (Figure 4.24).

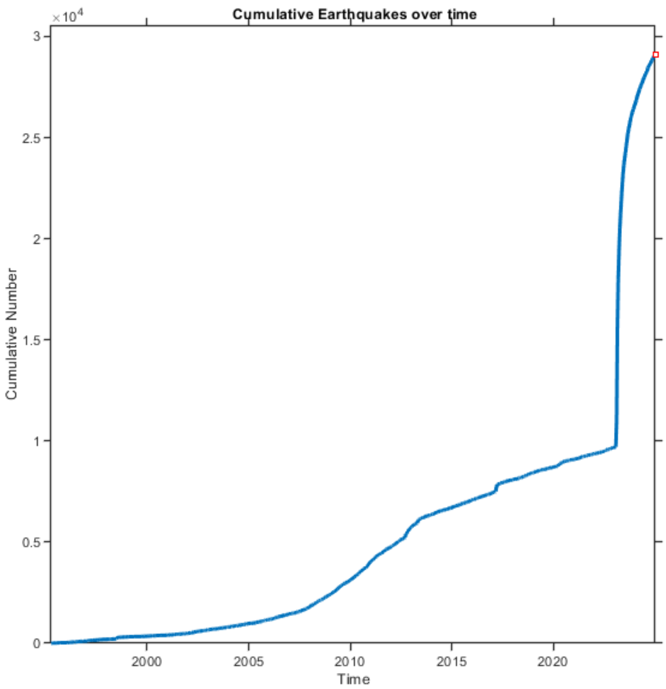

Figure 4.24. Total number of earthquakes recorded from 1995 to 2024.

The general background seismicity of the region was examined. After declustering and excluding events deeper than 40 km from the catalog, 18020 events were used to compute the spatial variations and temporal changes of b-values related to the background seismicity of the region. The spatial variation of b-values ranged between 0.6 and 1.5. The b-values result from 1995 to 2024 illustrate that areas near the epicenter of the mainshock exhibit high b-values. Similarly, the region near the epicenter of the second shock (particularly around Sürgü, Çardak, and the Göksun bend) shows elevated b-values. The Hatay region displays generally high b-values; however, its southern and southwestern parts exhibit lower values. The Gulf of İskenderun and its northeastern surroundings, especially near the Düziçi-İskenderun fault zones and the Kilis-Gaziantep region, are characterized by low b-values. Additionally, the area where the EAF splits into its northern strand, near Çelikhan, also shows low b-values (Figure 4.25).

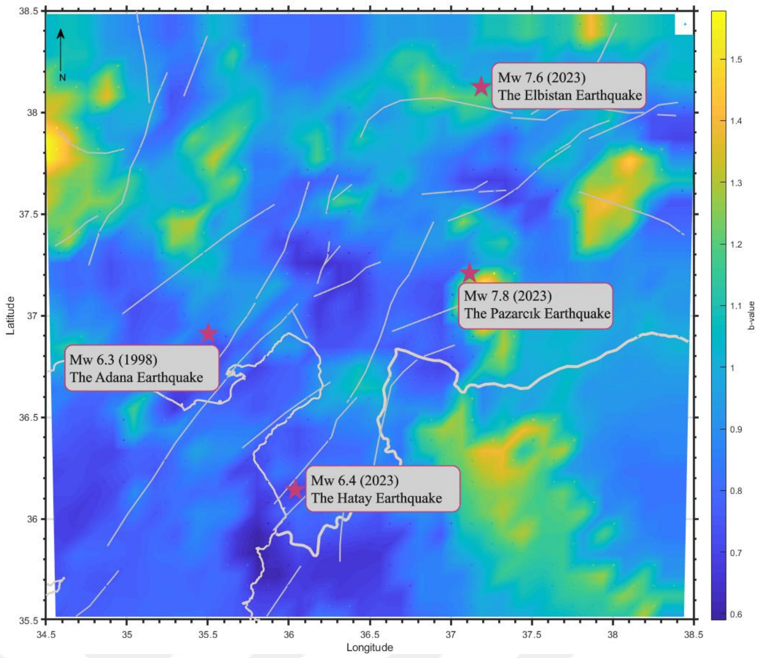

Figure 4.25. The spatial variation of b-value between 1995 and 2024. Pink stars represent the epicenter of earthquakes.

The temporal changes in the b-values were calculated for each sample containing 300 events, with a shifting step of 50 events. Although it shows fluctuations, the b-value reached its lowest value of 0.58 before the doublet earthquakes in 2023 (Figure 4.26).

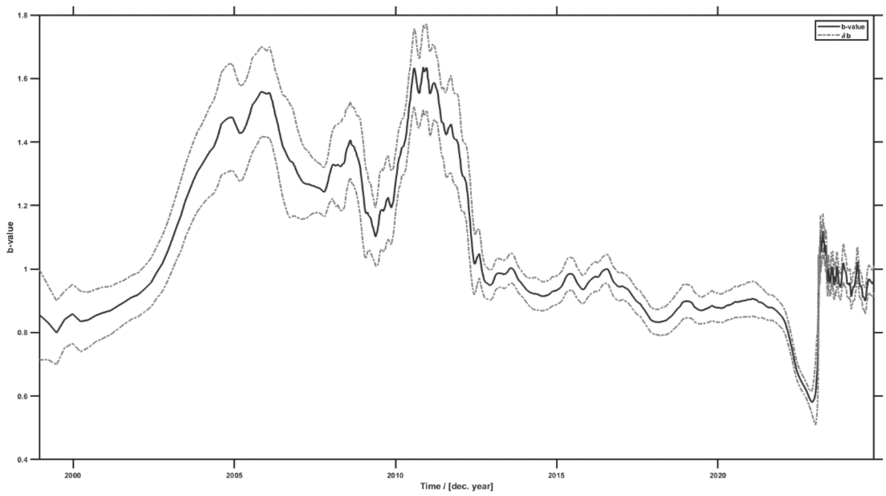

Figure 4.26. The temporal changes in the b-values for the time period between 1995 and 2024.

4.3. Coseismic Deformation Pattern

The coseismic deformation was analyzed by the Insar Technique in order to understand the deformation caused by the 2023 double earthquakes in the region. The Insar Scientific Computing Environment (ISCE) software was used to generate interferogram (Rosen et al., 2012). ISCE, developed by NASA's Jet Propulsion Laboratory and Stanford University, is a Python-based framework designed for processing SAR data from various satellite platforms, including RADARSAT, Sentinel-1 and ALOS. It supports both Terrain Observation with Progressive Scans (TOPS) and Stripmap acquisition modes. Sentinal-1 data were used in this study and obtained through the Alaska Satellite Facility (ASF) Data Search portal. The interferogram was generated in TOPS mode. The ascending image pair corresponds to path 14 and frame 119. The primary and secondary satellite images were obtained on 28 January 2023 and 9 February 2023, respectively, with a temporal baseline of 12 days. A multilook factor of 21:9 was applied in the range and azimuth direction to reduce noise. A coherence threshold of 0.3 was used to mask low-quality pixels. Interferogram unwrapping was performed by applying the minimum cost flow algorithm implemented in the SNAPHU software (Chen and Zebker, 2000).

The InSAR data covering the region between 36°-39°N Latitude and 34°-38°E Longitude were used to investigate surface deformation caused by the 2023 doublet earthquakes. Sentinel-1 image pairs were carefully selected from dates before and after the earthquake sequence to capture the coseismic deformation patterns across the region. The observed fringes represent changes in the radar phase resulting from ground displacement. The concentric and continuous nature of the fringes indicates a high level of ground deformation. The interferogram highlights multiple zones of significant displacement and exhibits broadly distributed deformation in the study area (Figure 4.27).

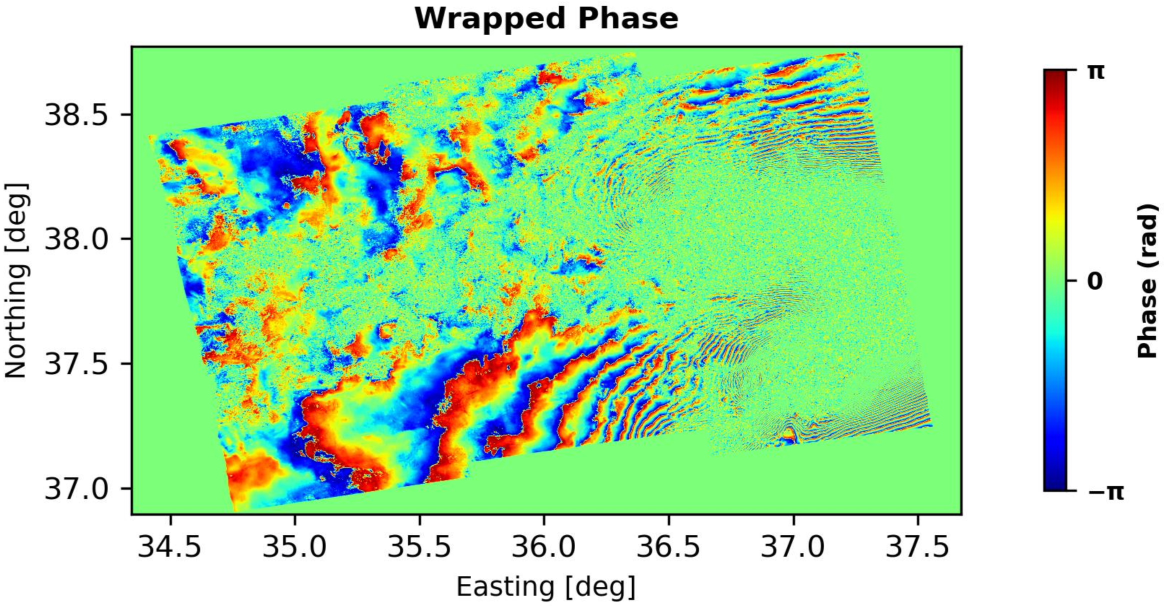

Figure 4.27. Wrapped interferogram showing coseismic deformation due to the February 2023 earthquakes.

5. DISCUSSION

The entire catalog from 1900 to 2024 was examined in detail to estimate the temporal changes and spatial variations in the b-value of the study region before and after the doublet earthquakes that occurred in 2023.

After examining the catalog from 1900 to 2024, a noticeable increase in seismic activity is observed around 1995 when determining the temporal period of Mc. The number of observed events throughout the period between 1900 and 1994 is significantly lower compared to the period between 1995 and 2024 (Figure 5.1).

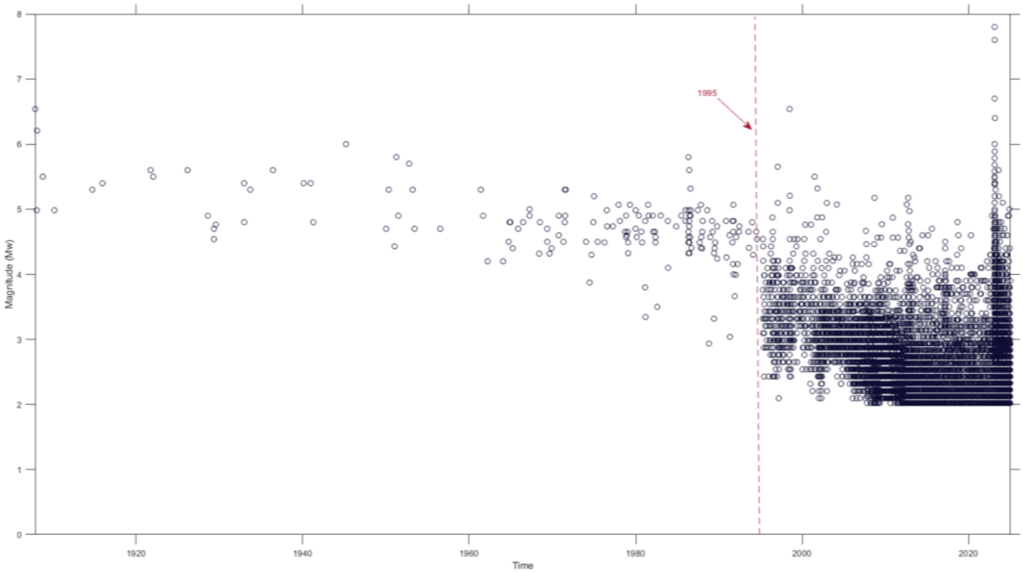

Figure 5.1. Magnitude versus time distributions of the earthquakes for the time period between 1900 and 2024.

The increase in the seismic activity after 1995 is largely due to the improved detection capabilities and the denser distribution of seismic networks (Öztürk, 2000; Tan, 2021). As mentioned earlier, the number of recorded events affects the fluctuation of Mc values over time. It is clearly seen that Mc values in the region exhibit a significant decrease from approximately 4.5 around 1995, and followed by a continued downward trend over time, reaching a value of 2. These fluctuations are consistent with the previous studies reported by Öztürk (2018; 2020), Akar (2024) and Sharma and Biswas (2025) for the variation of Mc in that region (Figure 5.2).

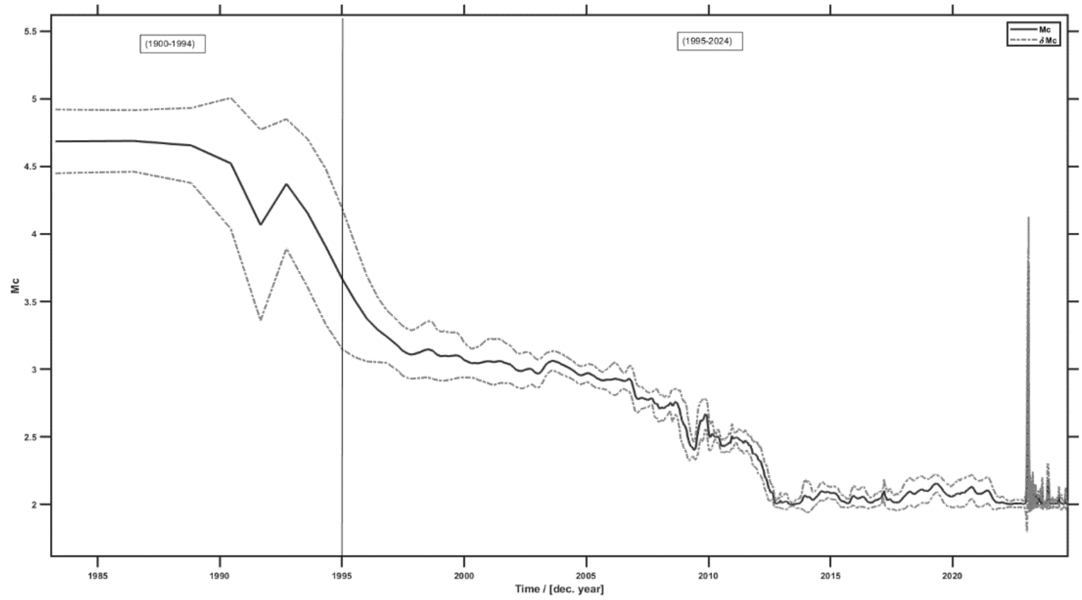

Figure 5.2. Temporal changes in magnitude of completeness for earthquakes in the study area during the period 1900-2024.

After determining the starting point of the catalog period, the years 1995–2024 were selected for the spatial and temporal analysis of the b-value in the region. Between 1995 and 2004, the Adana Basin exhibited relatively high b-values which are likely attributable to the released stress by the 1998 Adana Earthquake. The region displays different seismicity in the period between 2005-2014, and 2014-2023, leading up to the mainshock. During 2005-2014, 5739 events were recorded in the region, whereas in the period of 2015-2023, 3008 events were recorded. Seismic activity decreased by nearly 50%. This reduction may suggest stress accumulation in the area. Additionally, during the 2015-2023 period, low b-values were observed between the epicenters of the doublet earthquakes. This clearly shows that b-value analysis can be used as indicator of potential large earthquakes.

Temporal variation of b-value for the period 1995-2024 shows that b-values ranged between 0.58 and 1.6. This range is consistent with the result of previous studies. For instance, Maden and Öztürk (2015) determined b-values in the range of 0.6-1.8, Bayrak et al. (2015) found values change in a range between 0.7-1.7, and Öztürk (2018) reported b-values varying from 0.66 to 1.60. A detail year-by-year investigations reveals that b-values fluctuated from 2004 to 2013, remaining above 1.1 until 2013. Following that, an important change was observed in the b-values, which decreased below 1.0 and remained low until 2021. Starting from 2021, it gradually decreased to 0.58, reaching its lowest point prior to the doublet earthquakes. Following these events, in the postseismic stage of the Kahramanmaraş earthquakes, the b-values began to increase again. These results align with those of Kwiatek et al. (2023), Akar (2024), Sharma and Biswas (2025), Rodríguez-Pérez and Zúñiga (2025).

After 2023 doublet earthquake, fault plane solutions, including the mainshocks and aftershocks with magnitudes of equal to or larger than 4.0, represent left-lateral strike-slip faulting mechanism. However, the earthquakes with normal and reverse components occurred in the region shows that the region is a tectonically complex area containing both compressional and extensional stress regimes as a result of the movements of the surrounding plates (please see Figure 2.5).

Crustal structure features of the EAF have been investigated in several studies using various techniques including tomography, seismic velocity (Vp/Vs), gravity and magnetic, and magnetotellurics studies (Türkoğlu et al., 2015; Karabulut et al., 2019; Özer et al., 2019; Medved et al., 2021; Ogden and Bastow, 2022). According to tomographic studies the crustal structure of the EAF is highly complex, reflecting active tectonic movements, small-scale faulting mechanism, and fractured zones. Previous studies have revealed heterogeneous 3D P- and S-wave velocity models, which helped to explain and support the observed b-value variability in the region (Salah et al., 2011; Özer et al., 2019; Medved et al., 2021). In simple terms, higher crustal heterogeneity is associated with higher b-values, meaning that these regions tend to experience small earthquakes relative to large ones. Conversely, more homogenous regions often exhibit lower b-values. This may explain the observed high b-values which is above 1.1 during the period from 2003 to 2013, as the region did not experience large earthquakes in that time frame and frequency of small earthquakes is higher.

Based on the geophysical studies mentioned above, crustal thickness in Eastern Anatolia is estimated to be approximately 45-50 km (Karabulut et al., 2019; Özer et al., 2019). This estimate aligns with the earthquake catalog data following the 2023 doublet earthquakes through the end of 2024, which shows seismic activity extending from to surface down to 39.4 km, with magnitudes between 2.0 and 7.8 Mw (Figure 5.3) (Figure 5.4).

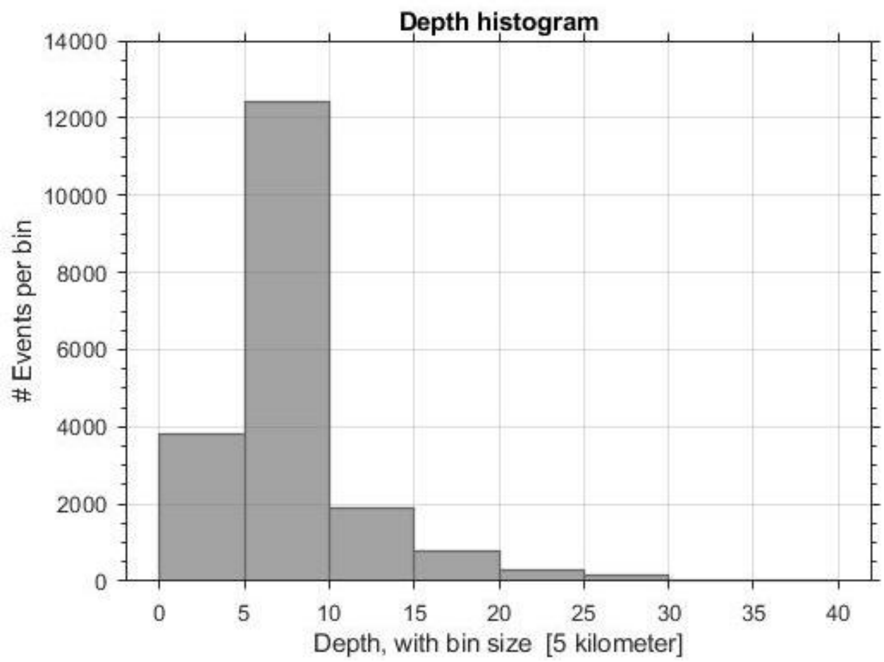

Figure 5.3. Number of events versus depth histogram for the time period between 2023 and 2024.

When comparing the spatial changes in b-values, it is observed that during the periods 2005-2014 and 2015-2023 (prior to the doublet earthquakes), b-values were lower ($b < 1$) in areas near the epicenters of the doublet earthquakes. Studies suggest that lower b-values represents the higher risk for future earthquakes. Low b-values are generally associated with high stress accumulation in a region, a relationship supported by both observational seismology and laboratory experiments. (Mogi, 1967; Scholz, 1968; Wyss, 1973; Nalbant et al., 2002; Aktuğ et al., 2013). Therefore, the occurrence of the doublet earthquakes may be interpreted as the release of stress that had gradually built up and accumulated over time in this region. For instance, in Türkiye, similar low b-value trends were identified prior to the 1999 İzmit Earthquake (Westerhaus et al., 2002), and the 2011 Van Earthquake (Görgün, 2013).

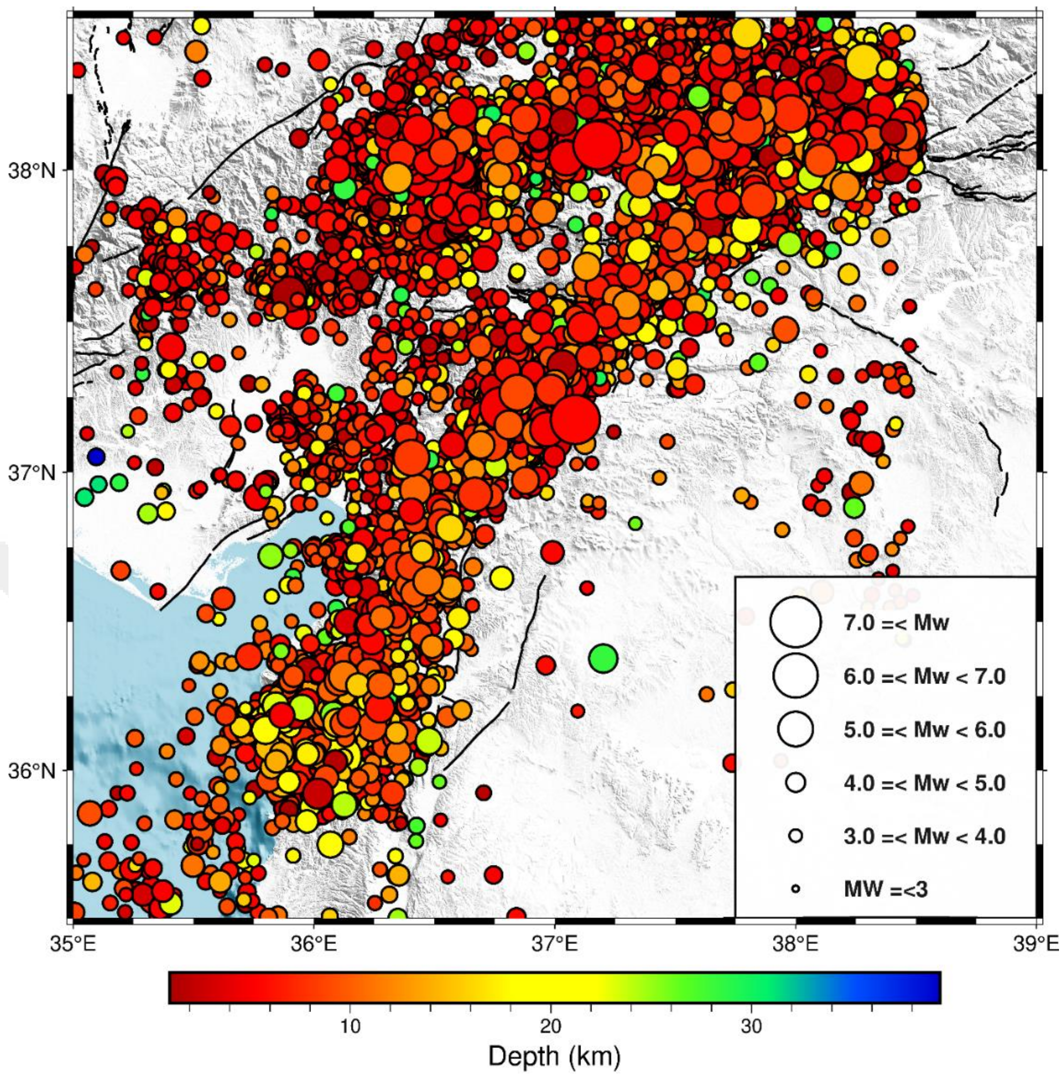

Figure 5.4. Depth distribution of earthquakes from the mainshock in 2023 and to the end of 2024.

During both the 2023-2024 and 1995-2024 periods, several areas exhibited relatively low b-values particularly northeast and southeast of the Gulf of Iskenderun toward Cyprus arc (Figure 4.22) (Figure 4.25). The 1995-2024 analysis further highlights additional zones of low b-values, including Düziçi-İskenderun fault zone, areas near Karataş Fault, the southern part of Hatay, namely northern part of the DSF, and the region between Gaziantep and Kilis. These low b-values may indicate increased stress accumulation in these areas, especially following the 2023 doublet earthquakes, as the regional stress field was significantly altered. Therefore, these regions require careful monitoring and should be considered priority areas for the future seismic hazard assessment.

When there are several fault systems in a fault zone, if an earthquake occurs, the energy can be transferred to surrounding faults. This occurrence is known as stress transfer, and it is referred to as triggering. To examine stress interaction and distribution within a fault zone, Coulomb stress analysis is often used. For example along the NAF, an earthquake sequence occurred between 1939 and 1999. These earthquakes took place in area where Coulomb stress had increased due to the previous ruptures (Stein et al., 1997). In this study, the first 10 earthquakes were examined to assess whether the second major shock in 2023 was promoted by the initial mainshock and to observe the stress distribution following that event magnitudes with Mw≥5. The result suggests that the second shock was likely caused by the main shock due to increased positive Coulomb stress observed in the northeast and northwest direction, around the second shock epicenter. Increased stress was also detected in the Hatay-Syria border to the south and in the Gulf of İskenderun to the southwest. The result is consistent with the previous study of Alkan et al. (2024), on the coulomb stress distribution along the EAF. Further the Coulomb analysis was conducted after the second shock, extending into 2024, to evaluate how the region's static stress evolved in the study area particularly to observe changes at the higher latitudes of the study region. The results also aligned with the study of Alkan et al. (2024). And final coulomb stress analysis for the 47 earthquakes was performed to present an improved depiction of the regional stress distribution. The results were consistent with previous studies on EAF (Stein et al., 2023; Alkan et al., 2024; Ma et al., 2025). The stress orientations in the map are similar; however, our calculated values are lower than those reported by Ma et al. (2025) and Stein et al. (2023), but are close to those of Alkan et al. (2024), likely due to differences in the input parameters. Moreover, their study examined earthquakes with magnitudes exceeding 5.9–6.0, our analysis encompassed events with magnitudes ≥5.0. The 1992 Landers Earthquake (Mw 7.3) triggered significant changes in the regional stress field, producing lobes of positive Coulomb stress on nearby faults. Approximately three hours later, the Big Bear Earthquake (Mw 6.5) occurred nearly 40 km west of the Landers rupture. Although located on a different fault system, the Big Bear event is widely considered a triggered aftershock, as the Landers rupture increased Coulomb stress in that area by over 2 bars, promoting failure on conjugate fault structures (Stein et al., 1994; King et al., 1994). Years later, the 1999 Hector Mine earthquake struck the north of the Landers rupture. Modeling showed that the Landers earthquake had increased the Coulomb stress at the Hector Mine hypocenter by approximately 0.5 bars (Parsons and Dreger, 2000). Studies suggested that post-seismic relaxation process further increased this stress over time, promoting the delayed rupture (Freed and Lin, 2001; Pollitz et al., 2001). These events provide example to the stress transfer and how positive Coulomb stress changes can trigger both aftershocks and large earthquakes on surrounding faults.

Aftershocks in these regions are well correlated with area of positive Coulomb stress change (Figure 4.11). It may be considered that aftershocks and possible future earthquakes are likely to take place in these zones of positive Coulomb stress change. Therefore, these positive zones should be given attention in future seismic hazard analyses.

The recurrence interval of earthquakes is a fundamental parameter in earthquake forecasting. It helps estimate the likelihood of future seismic events by identifying how often large earthquakes have occurred in the past. When combined with geological, geodetic, and historical data, recurrence intervals contribute to probabilistic seismic hazard models that guide risk assessment.

Accurately determining recurrence intervals for the northern strand of the EAF remains challenging due to the limited availability of paleoseismological data. For example, Duman et al. (2020) presented the first paleoseismological findings for northern strands of the EAF, including Karataş, Yumurtalık, Toprakkale, Düziçi-İskenderun faults. Their investigations, based on sedimentological and structural evidence, indicate that these faults have resulted in surface-rupturing events during the Holocene. They suggest that these faults have the potential of generating large surface-rupture earthquakes and can also rupture together in complex, multi-segmented events, such as the AD 242 event, which was detected on the Yumurtalık, Karataş and Düziçi-İskenderun segments. Since the AD 242 event, 1.7 meters of stress have built up on Karataş and Yumurtalık fault segments determined by an estimated slip rate of roughly 1 mm/yr (Duman and Emre, 2013; Duman et al., 2020). For the Düziçi-İskenderun fault segments, less than 1 meter of stress has accumulated, corresponding to slip rates below 1 mm/yr (Duman et al., 2020). The Gulf of İskenderun, one of the most highly industrialized areas of the Eastern Mediterranean, contains active seismic faults. As demonstrated by the 7.6 Mw earthquake in 2023 on the Çardak fault, low slip rates and long recurrence intervals should not be underestimated when assessing seismic risk. In this study, the results of both b-value and Coulomb stress analyses are consistent, highlighting the seismic potential of this region and emphasizing the need for greater attention to future earthquake risk.

Geodetic observations particularly derived from GPS and InSAR data, are crucial for understanding the crustal deformation. These techniques measure ground motion with millimeter-level precision, capturing the accumulated strain along fault zones. Strain rate analysis derived from geodetic data helps to identify regions where tectonic stress accumulates. Özbey et al. (2024) utilized a continuous velocity field interpolation method to determine the strain rate tensors of the Eastern Mediterranean for the interseismic period of the 2023 earthquakes (Figure 5.5). The region encompassing the Gulf of İskenderun and the Düziçi-Osmaniye area, particularly southern part of the EAF and the western segments of the SMF system, exhibits notable strain accumulation, with values reaching up to 30 nanostrain/yr. The Gulf of İskenderun is characterized by overlapping high-strain zones indicating a significant potential for future large earthquakes. These findings align with our study, particularly in the regions highlighted for their seismic risk potential.

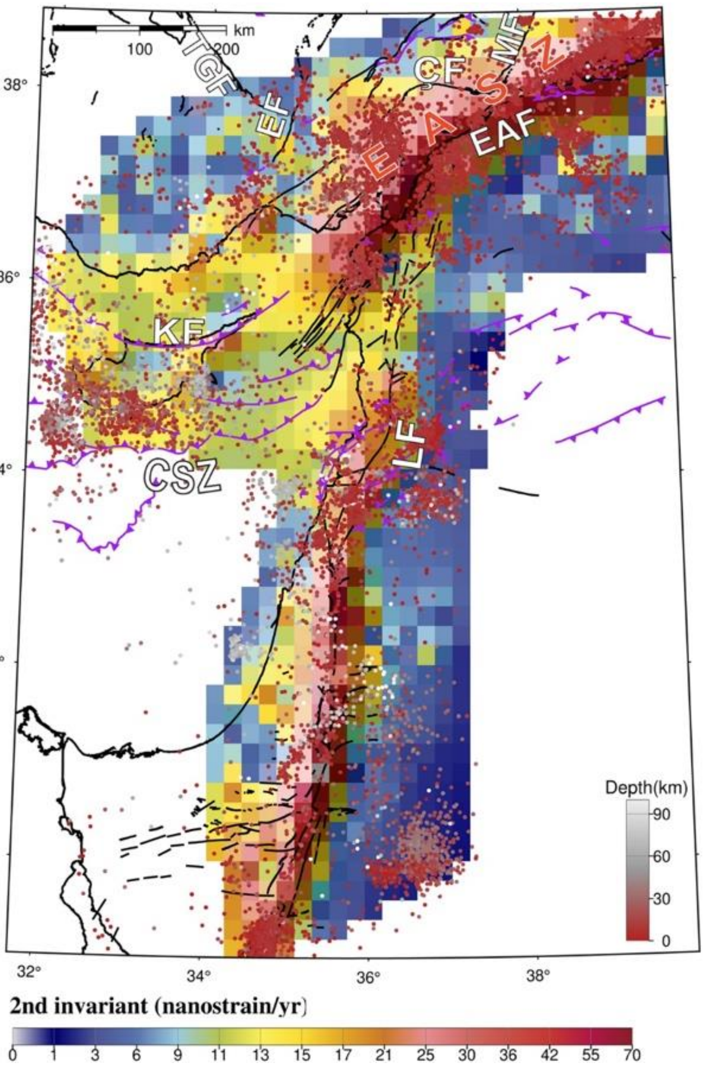

Figure 5.5. The second invariant of strain rate tensor (retrieved from Özbey et al., 2024) (Abbreviations used in map; CSZ: Cyprus Subduction Zone, ÇF: Çardak Fault, EAF: East Anatolian Fault, EASZ: East Anatolian Shear Zone, EF: Ecemiş Fault, KF: Kyrenia Fault, LF: Levant Fault, MF: Malatya Fault, TGF: Tuz Gölü Fault).

Moreover, Cheloni et al. (2025) investigated the interseismic strain accumulation along the EAF by adopting the Shen et al. (2015) algorithm which applies optimal interpolation of the spatially discretized geodetic data. They examined GNSS data from a network of 836 stations provided by the study of Kurt et al. (2023), to calculate the strain rate. The data covered the years from 1992 to 2020. According to their results, strain rates can reach up to 70 nanostrain/yr along the EAF (Figure 5.6). The area near the Gulf of İskenderun exhibits high strain rates particularly around Karataş, Düziçi-Osmaniye, and

Hatay regions. These findings also highlight high-risk zones and are consistent with our results, which emphasize the same areas as regions of elevated seismic risk with low b-values and positive stress change.

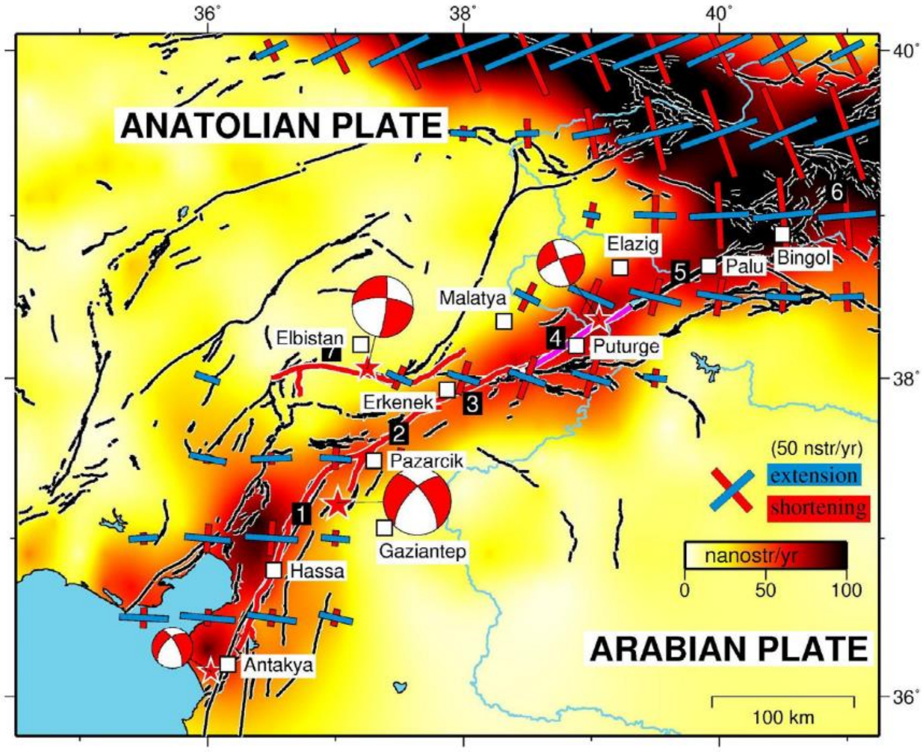

Figure 5.6. The second invariant of the strain-rate tensor (captured from Cheloni et al., 2025).

Erdik et al. (2023) also investigated the strain rate tensor to examine regional deformation patterns using GPS data. For this purpose, they utilized the comprehensive dataset compiled by Palano et al. (2017), which was developed by reprocessing earlier GPS measurements reported by Hessami et al. (2006), Reilinger et al. (2006), Walpersdorf et al. (2006), Masson et al. (2007), Tavakoli et al. (2008), Peyret et al. (2009), Djamour et al. (2011), Mousavi et al. (2013), Zarifi et al. (2013), and Walpersdorf et al. (2014). Utilizing the interpolation algorithm developed by Shen et al. (2015), they calculated the strain rate tensor to investigate the deformation pattern (Figure 5.7). Their findings indicate that the area surrounding Osmaniye has relatively high strain rates and clearly indicating ongoing strain accumulation, similar to those reported by Özbey et al. (2024) and Cheloni et al. (2025).

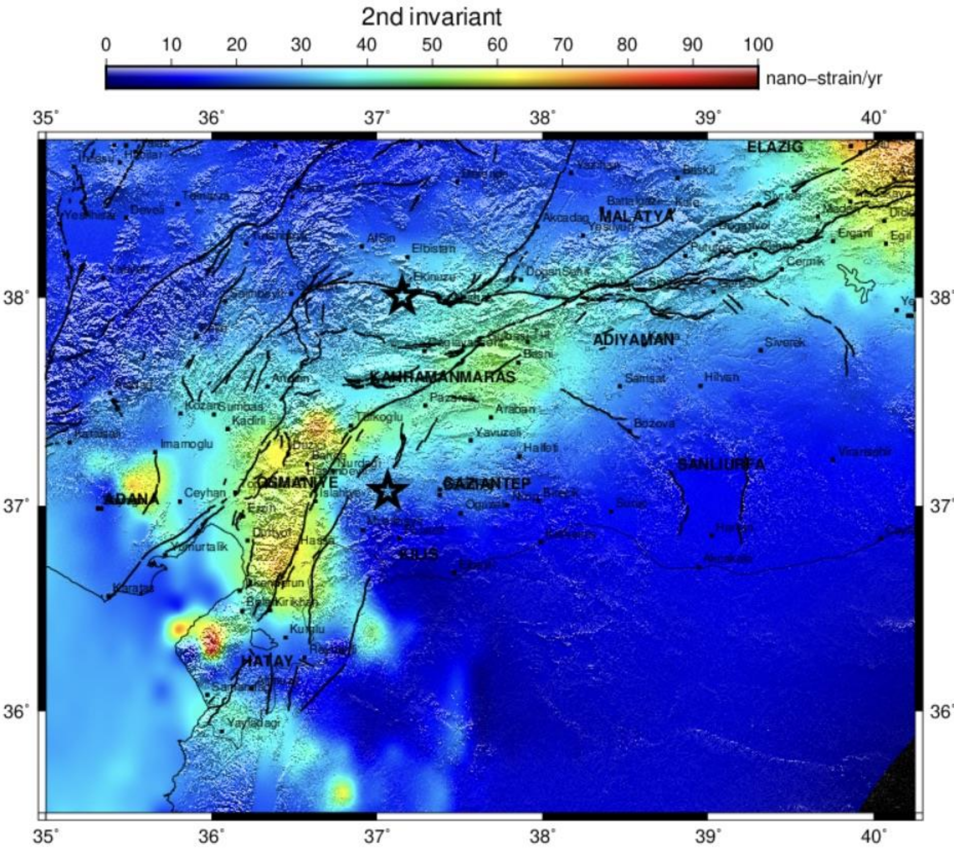

Figure 5.7. The second invariant strain rates around the EAF (captured from Erdik et al., 2023).

Interseismic strain analyses indicate that these regions are characterized by high strain rates and increased tectonic loading. It is suggested that stress is accumulating over time. After the 2023 doublet earthquakes, further investigations using b-value analysis and Coulomb stress modeling revealed that several of these same areas exhibit low b-values and positive Coulomb stress changes. Morever, InSAR coseismic analysis provides additional evidence by detecting significant deformation in these regions, reinforcing the interpretation that highlighted regions are under considerable tectonic stress (Please see Figure 4.27). The spatial overlap among areas of high strain rate, positive Coulomb stress change, low b-values, and notable surface deformation indicates a consistent pattern of increased seismic hazard potential. Given this convergence of independent geophysical and geodetic indicators, these highlighted regions must be closely monitored and considered priority areas in future seismic hazard assessments.

6. CONCLUSION

The spatio-temporal analysis of the b-value was performed over a long time period from 1995 to the end of 2024 for the region between the 2023 earthquake doublet on the EAF. In addition to the b-value analysis, the Coulomb stress change analysis was conducted within the same area. InSAR technique was also utilized to observe coseismic deformation pattern in the study area. Based on the results of the analyses and calculations, this study highlights the following key implications:

(i) Historical earthquakes and instrumental period earthquakes are located along the main strand, the northern strand of the EAF, northern part of the DSF within the study area. These findings indicate that the region has a high level of tectonic activity.

(ii) Fault plane solutions represent that the region has not only pure strike-slip faulting mechanism, but also it has reverse and normal faulting mechanisms. It shows that the region is a tectonically complex area with both compressional and extensional stress regimes, as a result of movements of the surrounding plates.

(iii) b-value analysis for the time period between 1995 and 2004 showed the average b-value and Mc as 0.93 ± 0.05 and 3.0, respectively.

(iv) During the time period of 2005-2014, the average b-value was found as 1.12 ± 0.04 with and Mc of 2.5 for the study region.

(v) For the time period from 2015 to 2023 (up to one day before the mainshock), the average b-value was calculated as 0.87 ± 0.02 and the Mc was 2.0.

(vi) The spatial distribution of b-values in 1995-2024 period illustrates that several regions may be at potential seismic risk in the future based on their background seismicity. These regions include the Düziçi–İskenderun Fault Zone, areas near the Karataş Fault, the southern part of Hatay (the northern segment of the DSF), the region between Gaziantep and Kilis, the Toprakkale fault, the region between Adana basin and Göksun bend (around Savrun Fault), and near Çelikhan.

(vii) The Coulomb stress analysis results confirmed that first mainshock in 2023, promoted to the second shock.

(viii) The combined Coulomb stress analysis demonstrated that stress predominantly increased in the northeast toward the Karlıova direction; in the west around the Göksun bend and nearby faults; in the south along the Düziçi-Iskenderun fault zones extending from the Gulf of Iskenderun toward Cyprus Arc; as well as between Gaziantep and Kilis, and the southern part of Hatay.

(ix) Coseismic deformation analysis reveals a broad and spatially variable pattern of ground displacement across the study area.

(x) The spatial overlap among areas of high strain rate, positive Coulomb stress change, low b-values, and notable surface deformation indicates a consistent pattern of increased seismic hazard potential.

The aim of this study is to understand seismic hazard potential of the study region and the stress distribution before and after the 2023 doublet earthquakes. Therefore, the Coulomb stress change was examined together with the spatial variations and temporal changes in b-values within a long period of time. In addition, strain rate analyses along the southern part of the EAF were reviewed to better understand ongoing deformation, and InSAR-based coseismic deformation was analyzed to directly observe surface displacements associated with the earthquake sequence. The outcomes of the study provide a comprehensive understanding of preseismic and postseismic stress evolution and active crustal deformation in the region. It also offers an essential input for seismic hazard assessments and contributes to efforts aimed at mitigating risk in the southern and the southwestern part of the EAF. Although the Coulomb stress change modeling, b-value and deformation analyses provide valuable insight into the relationship between stress transfer, earthquake occurrence and seismic hazard assessment, relying only on these three techniques is not sufficient to forecast seismic events in the future. Therefore, a combination of several methods such as geodetic monitoring, paleoseismology, time-dependent probabilistic seismic hazard assessment, machine learning and artificial intelligence should be taken into consideration for the effective understanding of the possible future earthquakes.

REFERENCES

AFAD, The Disaster and Emergency Management Authority (AFAD) Earthquake Catalog. https://deprem.afad.gov.tr, accessed on January 10, 2025.

Akar, F., 2024, "Spatio-temporal changes in b-value associated with the 2023 Türkiye earthquake", *Journal of Earth System Science,* Vo1. 133, No. 4, 185.

Aki, K., 1965, "Maximum likelihood estimate of b in the formula log N = a - bM and its confidence limits", *Bulletin of the Earthquake Research Institute, Tokyo University*, Vol. 43, pp. 237–239.

Aktar, M. T., M. Ergin, S. Özalaybey, M. C. Tapırdamaz, A. Yorük, and F. Biçmen, 2000, "A lower-crustal event in the northeastern Mediterranean: The 1998 Adana earthquake (Mw = 6.2) and its aftershocks", *Geophysical Research Letters,* Vol. 27, No. 14, pp. 2361–2364.

Aktuğ, B., U. Dikmen, A. Dogru, and H. Ozener, 2013, "Seismicity and strain accumulation around Karliova Triple Junction (Turkey).", *Journal of Geodynamics,* Vol. 67, pp. 21–29.

Aktuğ, B., H. Ozener, A. Dogru, A. Sabuncu, B. Turgut, K. Halicioglu, O. Yilmaz and E. Havazli, 2016, "Slip rates and seismic potential on the East Anatolian Fault System using an improved GPS velocity field.", *Journal of Geodynamics*, Vol. 94-95, pp. 1–12.

Ali, S. M., and M. F. Akkoyunlu, 2022, "Statistical analysis of earthquake catalogs for seismic hazard studies around the Karliova Triple Junction (eastern Turkey)", *Journal of African Earth Sciences*, Vol. 186, 104436.

Alkan, H., S. Öztürk, and İ. Akkaya, 2023, "Seismic hazard implications in and around the Yedisu seismic gap (Eastern Türkiye) based on Coulomb stress changes, b-values, and S-wave velocity", *Pure and Applied Geophysics*, Vol. 180, No. 9, pp. 3227-3248.

Alkan, H., A. Büyüksaraç, and Ö. Bektaş, 2024, "Investigation of earthquake sequence and stress transfer in the Eastern Anatolia Fault Zone by Coulomb stress analysis", *Turkish Journal of Earth Sciences*, Vol. 33, No. 1, pp. 56–68.

Amelung, F., and G. King, 1997, "Earthquake scaling laws for creeping and non-creeping faults", *Geophysical Research Letters*, Vol. 24, No.5, pp. 507–510.

Amorèse, D., 2007, "Applying a change-point detection method on frequency-magnitude distributions", *Bulletin of the Seismological Society of America*, Vol. 97, No. 5, pp. 1742–1749.

Arpat, E. and F. Şaroğlu, 1972, "The East Anatolian Fault System; Thoughts on its Development", *Bulletin of the Mineral Research and Exploration*, Vol. 78, No. 78, pp. 1-12.

Arpat, E. and Şaroğlu, F., 1975, "Türkiye'deki bazı önemli genç tektonik olaylar", *Türkiye Jeoloji Kurumu Bülteni*, Vol. 18, No. 1, pp. 91-101.

Barbot, S., H. Luo, T. Wang, Y. Hamiel, O. Piatibratova, M. T. Javed, C. Braitenberg, and G. Gürbüz, 2023, "Slip distribution of the February 6, 2023 Mw 7.8 and Mw 7.6 Kahramanmaraş, Turkey earthquake sequence in the East Anatolian Fault Zone," *Seismica*, Vol. 2, No. 3, pp. 1–17.

Barka, A. A., and K. Kadinsky-Cade, 1988, "Strike-Slip Fault Geometry in Turkey and Its Influence on Earthquake Activity", *Tectonics*, Vol. 7, No. 3, pp. 663–684.

Barka, A. and R. Reilinger, 1997, "Active tectonics of the Eastern Mediterranean region: Deduced from GPS, neotectonic and seismicity data", *Annali Di Geofisica*, Vol. 40, No. 3, pp. 587–610.

Bayrak, E., Yılmaz, Ş., Softa, M., Türker, T., and Bayrak, Y., 2015, "Earthquake hazard analysis for East Anatolian fault zone, Turkey", *Natural Hazards,* Vol. 76, No.2, pp. 1063-1077.

Bird, P., 2003, "An updated digital model of plate boundaries", *Geochemistry, Geophysics, Geosystems*, Vol. 4, No. 3, 1027.

Bozkurt, E., 2001, "Neotectonics of Turkey–a synthesis", *Geodinamica acta,* Vol. 14, No.1-3, pp. 3-30.

Cao, A., and S. Gao, 2002, "Temporal variation of seismic b-values beneath northeastern Japan island arc", *Geophysical Research Letters,* Vol. 29, No. 9, pp. 481–483.

Cheloni, D., N. A. Famiglietti, A. Akinci, R. Caputo, A. Vicari, 2025, "Modeling the 2023 Türkiye Earthquakes and Strain Accumulation Along the East Anatolian Fault Zone: Insights from InSAR, GNSS, and Small-Magnitude Seismicity, with Implications for the Seismic Potential at Rupture Terminations", *Remote Sensing,* Vol. 17, No. 13.

Chen, C. W., and H. A. Zebker, (2000). Network approaches to two-dimensional phase unwrapping: intractability and two new algorithms. *Journal of the Optical Society of America A*, Vol. 17, No. 3, pp. 401-414.

Chorowicz, J., P. Luxey, N. Lyberis, J. Carvalho, J. F. Parrot, T. Yürür and N. Gündoğdu, 1994, "The Maras Triple Junction (southern Turkey) based on digital elevation model and satellite imagery interpretation", *Journal of Geophysical Research: Solid Earth*, Vol. 99, No. B10, pp. 20225-20242.

Console, R., M. Murru, and A. M. Lombardi, 2003, "Refining earthquake clustering models", *Journal of Geophysical Research: Solid Earth,* Vol. 108, No. B10.

D'Alessandro, A., D. Luzio, G. D'Anna, and G. Mangano, 2011, "Seismic Network Evaluation through Simulation: An Application to the Italian National Seismic

Network", *Bulletin of the Seismological Society of America,* Vol. 101, No. 3, pp. 1213–1232.

Dewey, J. F., M.R. Hempton, W. S. F. Kidd, F. Şaroglu, and A. M. C. Şengör, 1986, "Shortening of continental lithosphere: the neotectonics of Eastern Anatolia—a young collision zone", *Geological Society, London, Special Publications*, Vol. 19, No.1, pp. 1-36.

Djamour, Y., P. Vernant, H. R. Nankali, F. Tavakoli, 2011, "NW Iran–Eastern Turkey present-day kinematics: results from the Iranian permanent GPS network", *Earth and Planetary Science Letters*, Vol. 307, No. 1–2, pp. 27–34.

Donner, R., V., Y. Zou, J. F. Donges, N. Marwan, and J. Kurths, 2010, "Recurrence networks—A novel paradigm for nonlinear time series analysis", *New Journal of Physics,* Vol. 12, 033025.

Duman, T. Y., and Ö. Emre, 2013, "The East Anatolian Fault: geometry, segmentation and jog characteristics", *Geological Society, London, Special Publications,* Vol. 372, pp. 495-529.

Duman, T. Y., H. Elmacı, S. Özalp, A. Kürçer, M. Kara, E. Özdemir, A. Yavuzoğlu, and Ç. Uygun Güldoğan, 2020, "Paleoseismology of the western Sürgü–Misis fault system: east Anatolian Fault, Turkey", *Mediterranean Geoscience Reviews*, Vol. 2, No. 3, pp. 411-437.

Durand, V., M. Bouchon, H. Karabulut, D. Marsan, and J. Schmittbuhl, 2013, "Link between Coulomb stress changes and seismic activation in the eastern Marmara sea after the 1999, Izmit (Turkey), earthquake", *Journal of Geophysical Research: Solid Earth*, Vol. 118, No. 2, pp. 681-688.

Emre, Ö., T. Y. Duman, S. Özalp, H. Elmacı, Ş. Olgun and F. Şaroğlu, 2013, "Active fault map of Turkey with explanatory text", *General directorate of mineral research and exploration special publication series, 30.*

Erdik, M., M. B. D. Tümsa, A. Pınar, E. Altunel, and A. C. Zülfikar, 2023, “A preliminary report on the February 6, 2023 earthquakes in Türkiye”, *Temblor*.

Freed, A. M., and J. Lin, 2001, “Earthquake triggering by static, dynamic, and postseismic stress transfer”, *Annual Review of Earth and Planetary Sciences,* Vol. 29, pp. 335–367.

Frohlich, C., and S. D. Davis, 1993, “Teleseismic b values; or, much ado about 1.0”, *Journal of Geophysical Research: Solid Earth,* Vol. 98, No. B1, pp. 631-644.

Gardner, J. K., and L. Knopoff, 1974, “Is the sequence of earthquakes in Southern California, with aftershocks removed, Poissonian?”, *Bulletin of the Seismological Society of America*, Vol. 64, No. 5, pp. 1363–1367.

Görgün, E., 2013, “Analysis of the b-values before and after the 23 October 2011 Mw 7.2 Van–Erciş, Turkey earthquake”, *Tectonophysics*, Vol. 603, pp. 213-221.

Gutenberg, B., and C. F. Richter, 1944, “Frequency of earthquakes in California”, *Bulletin of the Seismological Society of America,* Vol. 34, No. 4, pp. 185–188.

Hanssen, R. F.**,** *Radar interferometry: Data interpretation and error analysis,* 2001.

Harris, R. A., 1998, “Introduction to special section: Stress triggers, stress shadows, and implications for seismic hazard. *Journal of Geophysical Research,* Vol. 103, No. B10, pp. 347– 358.

He, L., G. Feng, W. Xu, Y. Wang, Z. Xiong, H. Gao, and X. Liu, 2023**,** “Coseismic kinematics of the 2023 Kahramanmaraş Turkey earthquake sequence from InSAR and optical data”, *Geophysical Research Letters,* Vol. 50, No.18.

Hempton, M. R., 1981, “The East Anatolian transform fault: Along-strike variations in geometry and behavior”, *Eos, Transactions American Geophysical Union*, Vol. 62, No. 17.

Hempton, M. R., 1987, “Constraints on Arabian plate motion and extensional history of the Red Sea”, *Tectonics*, Vol.6, No. 6, pp. 687-705.

Hessami, K., F. Nilforoushan, C. J. Talbot, 2006, “Active deformation within the Zagros Mountains deduced from GPS measurements”, *Journal of the Geological Society*, Vol. 163, No. 1, pp. 143–148.

Jackson, J., and D. McKenzie, 1984, “Active tectonics of the Alpine—Himalayan Belt between western Turkey and Pakistan”, *Geophysical Journal International*, Vol. 77, No. 1, pp. 185-264.

KOERI, *Boğaziçi University Kandilli Observatory Earthquake Research Institute, BDTIM Earthquake Query System*, http://www.koeri.boun.edu.tr/sismo/, accessed on January 10, 2025.

Karabulut, H., A. Paul, D. Cambaz, A. Kömeç Mutlu, D. Aksarı, and T. A. Ergün (2019). The images of Anatolia. *EGU General Assembly*, 12–17 April 2019, Vienna, Austria.

Ketin, İ., 1966, “Anadolu'nun tektonik birlikleri”, *Bulletin of the Mineral Research and Exploration*, Vol. 66, No. 66, pp. 20-37.

King, G. C., R. S. Stein, and J. Lin, 1994, “Static stress changes and the triggering of earthquakes”, *Bulletin of the Seismological Society of America*, Vol. 84, No. 3, pp. 935-953.

Koç, A., and N. Kaymakcı, 2013, “Kinematics of Sürgü fault zone (Malatya, Turkey): A remote sensing study”, *Journal of Geodynamics*, Vol. 65, pp. 292-307.

Koçyiğit, A., and A. A. Özacar, 2003, “Extensional neotectonic regime through the NE edge of the outer Isparta Angle, SW Turkey: New field and seismic data”, *Turkish Journal of Earth Sciences*, Vol. 12, No. 1, pp. 67–90.

Kwiatek, G., P. Martínez-Garzón, D. Becker, G. Dresen, F. Cotton, G. C. Beroza, U. Acar, S. Ergintav, M. Bohnhoff, 2023, "Months-long seismicity transients preceding the 2023 Mw 7.8 Kahramanmaraş earthquake, Türkiye", *Nature Communications,* Vol. 14, No. 1, 7534.

Lin, J., and R. S. Stein, 2004, "Stress triggering in thrust and subduction earthquakes, and stress interaction between the southern San Andreas and nearby thrust and strike-slip faults", *Journal of Geophysical Research: Solid Earth,* Vol. 109, B02303.

Lin, J., J. Sibuet, C. Lee, S. Hsu, and F. Klingelhoefer, 2007, "Spatial variations in the frequency–magnitude distribution of earthquakes in the southwestern Okinawa Trough", *Earth, Planets and Space,* Vol. 59, pp. 221–225.

Ma, X., Y. Liu, and Z. Chen, 2025, "Space–Time Stress Variations near the East Anatolian Fault Zone and the Triggering Relationship of Earthquakes", *Applied Science,* Vol. 15, No. 5.

Mai, P. M., T. Aspiotis, T. A. Aquib, E. V. Cano, D. Castro-Cruz, A. Espindola-Carmona, B. Li, X. Li, J. Liu, R. Matrau, A. Nobile, K. H. Palgunadi, M. Ribot, L. Parisi, C. Suhendi, Y. Tang, B. Yalcin, U. Avşar, Y. Klinger, and S. Jónsson, 2023, "The destructive earthquake doublet of 6 February 2023 in South-Central Türkiye and Northwestern Syria: Initial observations and analyses", *The Seismic Record,* Vol. 3, No. 2, pp. 105–115.

Maden, N., and S. Öztürk, 2015, "Seismic b-values, bouguer gravity and heat flow data beneath Eastern Anatolia, Turkey: Tectonic implications", *Surveys in Geophysics,* Vol. 36, No. 4, pp. 549-570.

Mahmoud Y., F. Masson, M. Meghraoui, Z.Cakir, A. Alchalbi, H. Yavasoglu, Ö. Yönlü, M. Daoud, S. Ergintav, S. Inan, 2013, "Kinematic study at the junction of the East Anatolian Fault and the Dead Sea Fault from GPS measurements", *Journal of Geodynamics,* Vol. 67, pp. 30–39.

Massonnet, D., and K. L. Feigl, 1998, "Radar interferometry and its application to changes in the Earth's surface", Reviews of Geophysics, Vol. 36, No. 4, pp. 441–500.

McClusky S., S. Balassanian, A. Barka, C. Demir, S. Ergintav, I. Georgiev, O. Gurkan, M. Hamburger, K. Hurst, H. Kahle, K. Kastens, G. Kekelidze, R. King, V. Kotzev, O. Lenk, S. Mahmoud, A. Mishin, M. Nadariya, A. Ouzounis, D. Paradissis, Y. Peter, M. Prilepin, R. Reilinger, I. Sanli, H. Seeger, A. Tealeb, M. N. Toksöz and G. Veis, 2000, "Global Positioning System constraints on plate kinematics and dynamics in the eastern Mediterranean and Caucasus", *Journal of Geophysical Research: Solid Earth*, Vol. 105, No. B3, pp. 5695-5719.

McKenzie, D., 1972, "Active tectonics of the Mediterranean region", *Geophysical Journal International*, Vol. 30, No. 2, pp. 109-185.

McKenzie, D., 1978, "Some remarks on the development of sedimentary basins", *Earth and Planetary Science Letters*, Vol. 40, No. 1, pp. 25–32.

Melgar, D., T. Taymaz, A. Ganas, B. W. Crowell, T. Öcalan, M. Kahraman, V. Tsironi, S. Yolsal-Çevikbilen, S. Valkaniotis, T. S. Irmak, T. Eken, C. Erman, B. Özkan, A. H. Dogan and C. Altuntaş, 2023, "Sub- and super-shear ruptures during the 2023 Mw 7.8 and Mw 7.6 earthquake doublet in SE Türkiye," *Seismica*, Vol. 2, No. 3, pp. 1–10.

Mignan, A., and J. Woessner, 2012, "Estimating the magnitude of completeness for earthquake catalogs", Community Online Resource for Statistical Seismicity Analysis, http://www.corssa.org., accessed on May 21, 2025.

Mogi, K., 1962, "Magnitude-frequency relation for elastic shocks accompanying fractures of various materials and some related problems in earthquakes", *Bulletin of the Earthquake Research Institute*, Vol. 40, No. 4, pp. 831–853.

Mogi, K. (1967). Earthquakes and fractures. *Tectonophysics*, Vol. 5, No. 1, pp. 35-55.

Mousavi, Z., A. Walpersdorf, R. T. Walker, F. Tavakoli, E. Pathier, H. Nankali, F. Nilforoushan, Y. Djamour, 2013, "Global Positioning System constraints on the active tectonics of NE Iran and the South Caspian region", *Earth and Planetary Science Letters*, Vol. 377–378, pp. 287–298.

Murru, M., C. Montuori, M. Wyss, and E. Privitera, 1999, "The locations of magma chambers at Mt. Etna, Italy, mapped by b-values", *Geophysical Research Letters,* Vol. 26, pp. 2553–2556.

Nalbant, S. S., J. McCloskey, S. Steacy, A. A. Barka, 2002**,** "Stress accumulation and increased seismic risk in eastern Turkey", *Earth and Planetary Science Letters*, Vol. 195, No. 3-4, pp. 291-298.

Ogata, Y., M. Imoto, and K. Katsura, 1991, "3-D spatial variation of *b*-values of magnitude–frequency distribution beneath the Kanto District, Japan", *Geophysical Journal International,* Vol. 104, No.1, pp. 135–146.

Ogata, Y., and K. Katsura, 1993, "Analysis of temporal and spatial heterogeneity of magnitude frequency distribution inferred from earthquake catalogues", *Geophysical Journal International*, Vol. 113, No. 3, pp. 727-738.

Ogden, C. S., and I. D. Bastow, 2022, "The crustal structure of the Anatolian Plate from receiver functions and implications for the uplift of the central and eastern Anatolian plateaus", *Geophysical Journal International,* Vol. 229, No. 2, pp. 1041–1061.

Okada, Y., 1992, "Internal deformation due to shear and tensile faults in a half-space", *Bulletin of the Seismological Society of America,* Vol. 82, No. 2, pp. 1018–1044.

Okay A. I., and O. Tüysüz 1999, "Tethyan sutures of northern Turkey", *Geological Society London Special Publications,* Vol. 156, No. 1, pp. 475-515.

Özbey, V., A. M. C. Şengör, P. Henry, M. S. Özeren, A. J. Haines, E. C. Klein, E. Tarı, C. Zabcı, K. Chousianitis, S. E. Güvercin, N. Öğretmen, 2024, "Kinematics of the

Kahramanmaraş triple junction and of Cyprus: evidence of shear partitioning", *BSGF - Earth Sciences Bulletin*, Vol. 195, No. 15.

Özer, C., M. Özyazıcıoğlu, E. Gök, and O. Polat, 2019, "Imaging the crustal structure throughout the East Anatolian Fault Zone, Turkey, by local earthquake tomography", *Pure and Applied Geophysics*, Vol. 176, No. 6, pp. 2235–2261.

Öztürk, S., 2018, "Earthquake hazard potential in the Eastern Anatolian Region of Turkey: Seismotectonic b and Dc-values and precursory quiescence Z-value", *Frontiers in Earth Science*, Vol. 12, pp. 215–236.

Öztürk, S., 2020, "A study on the variations of recent seismicity in and around the Central Anatolian region of Turkey", *Physics of the Earth and Planetary Interiors*, Vol. 304, 106453.

Parsons, T., R. S. Stein, R. W. Simpson and P. A. Reasenberg, 1999, "Stress sensitivity of fault seismicity: A comparison between limited-offset oblique and major strike-slip faults", *Journal of Geophysical Research: Solid Earth*, Vol. 104, pp. 20183–20202.

Parsons, T., and D. S. Dreger, 2000, "Static-stress impact of the 1992 Landers earthquake sequence on nucleation and slip at the site of the 1999 M = 7.1 Hector Mine earthquake, southern California", *Geophysical Research Letters*, Vol. 27, No. 16, pp. 2381–2384.

Peyret, M., F. Masson, J. Martinod, F. Tavakoli, A. Walpersdorf, H. Nankali, S. Van Gorp, 2009, "Present-day strain distribution across the Minab-Zendan-Palami fault system from dense GPS transects", *Geophysical Journal International*, Vol. 179, No. 2, pp. 751–762.

Palano, M., P. Imprescia, A. Agnon, and S. Gresta, 2017, "An improved evaluation of the seismic/geodetic deformation-rate ratio for the Zagros Fold-and-Thrust collisional belt," *Geophysical Journal International*, Vol. 213, pp. 194–209.

Polat, G., 2022, "Spatial analysis of b-value variability in Elazig city and the surrounding area (Eastern Turkey)", *Acta Geophysica*, Vol. 70, No. 1, pp. 15-25.

Pollitz, F. F., I. S. Sacks, and W. Thatcher, 2001, "Effects of the 1992 Landers and 1995 Kobe earthquakes on the motion of the Pacific plate", *Nature*, Vol. 399 No. 6733, pp. 149–152.

Reasenberg, P., 1985, "Second-order moment of central California seismicity, 1969–1982", *Journal of Geophysical Research: Solid Earth*, Vol. 90, No. B7, pp. 5479-5495.

Reilinger, R., S., McClusky, P., Vernant, S., Lawrence, S., Ergintav, R., Cakmak, H., Ozener, F., Kadirov, I., Guliev, R., Stepanyan, M., Nadariya, G., Hahubia, S., Mahmoud, K., Sakr, A., ArRajehi, D., Paradissis, A., Al-Aydrus, M., Prilepin, T., Guseva, G., Karam, 2006, "GPS constraints on continental deformation in the Africa-Arabia-Eurasia continental collision zone and implications for the dynamics of plate interactions.", *Journal of Geophysical Research: Solid Earth*, Vol. 111, No. 5.

Rodríguez-Pérez, Q., and F. R. Zúñiga, 2025, "Statistical and source characterization of the 2023 Kahramanmaraş Türkiye earthquake sequence", *Acta Geophysica*, Vol. 73, No. 4, pp. 1241–1260.

Rosen, P. A., E. Gurrola, G. F. Sacco, and H. Zebker, 2012, "The InSAR Scientific Computing Environment", In *EUSAR 2012; 9th European Conference on Synthetic Aperture Radar*, pp. 730–733.

Rydelek, P. A., and I. S. Sacks, 1989, "Testing the completeness of earthquake catalogs and the hypothesis of self-similarity", *Nature*, Vol. 337, pp. 251–253.

Salah, M. K., A. I. Al-Lazki, and A.M. Al-Amri, 2011**,** "Seismic velocity and Poisson's ratio tomography of the crust beneath eastern Anatolia, Turkey", *Journal of Asian Earth Sciences*, Vol. 40, No. 6, pp. 746–761.

Sharma, V., and R. Biswas, 2025, “Seismic quiescence and b-value anomalies preceding the 6th February 2023 earthquake doublet (Mw 7.8, Mw 7.6) in Kahramanmaraş, Türkiye: A comprehensive analysis of seismic parameters along the East Anatolian Fault Zone”, *Acta Geophysica*, Vol. 73, pp. 1159–1185.

Scholz, C. H., 1968, “The frequency-magnitude relation of microfracturing in rock and its relation to earthquakes”, *Bulletin of the seismological society of America*, Vol. 58, No.1, pp. 399-415.

Scholz, C.H., “*The Mechanics of Earthquakes and Faulting”*, Second Edition, Cambridge University Press, Cambridge, 2002.

Schorlemmer, D., S. Wiemer, M. Wyss, 2004, “Earthquake statistics at Parkfield: 1. Stationarity of b values”, *Journal of Geophysical Research: Solid Earth*, Vol. 109. B12.

Schorlemmer, D., and J. Woessner, 2008, “Probability of detecting an earthquake”, *Bulletin of the Seismological Society of America*, Vol. 98, No. 5, pp. 2103–2117.

Shen, Z.-K., M. Wang, Y. Zeng, and F. Wang, 2015, “Optimal interpolation of spatially discretized geodetic data,” *Bulletin of the Seismological Society of America*, Vol. 105, No.4, pp. 2117–2127.

Stein, R. S., J. Lin, and G. C. P. King, 1994, “Stress triggering of earthquakes: Evidence for the 1994 M = 6.7 Northridge, California, shock”, *Annals of Geophysics*, Vol. 37, No. 6.

Stein, R. S., A. A. Barka, and J. H. Dieterich, 1997, “Progressive failure on the North Anatolian Fault since 1939 by earthquake stress triggering”, *Geophysical Journal International*, Vol. 128, No. 3, pp. 594–604.

Stein, R. S., S. Toda, A. D. Özbakır, V. Sevilgen, H. Gonzalez-Huizar, G. Lotto, and S. Sevilgen, 2023, “Interactions, stress changes, mysteries, and partial forecasts of the 2023 Kahramanmaraş, Türkiye, earthquakes”, *Temblor.*

Stiphout, T., J. Zhuang, and D. Marsan, 2012, “Seismicity declustering”, Community Online Resource for Statistical Seismicity Analysis, http://www.corssa.org., accessed on June 21, 2025.

Şaroğlu, F., 1985, “*Doğu Anadolu’nun neotektonik dönemde jeolojik ve yapısal evrimi”*, PhD Thesis, Istanbul University.

Şengör, A. M. C., 1979, “The North Anatolian transform fault: its age, offset and tectonic significance.”, *Journal of the Geological Society*, Vol. 136, No. 3, pp. 269-282.

Şengör, A. M. C., 1980, “Türkiye’nin neotektoniğinin esasları”, *Türkiye Jeoloji Kurumu Konferans Serisi*, Ankara.

Şengör, A. C., and Y. Yilmaz, 1981, “Tethyan evolution of Turkey: a plate tectonic approach”, *Tectonophysics*, Vol. 75, No. 3-4, pp. 181-241.

Şengör, A. C., and N. Canitez, 1982, “The North Anatolian Fault.”, *Alpine-Mediterranean Geodynamics*, Vol.7, pp. 205-216.

Şengör, A. M., N. Görür, and F. Şaroğlu, 1985, “Strike-Slip Faulting and Related Basin Formation in Zones of Tectonic Escape: Turkey as a case study”, *Strike-Slip Deformation, Basin Formation, and Sedimentation*, Vol. 37, pp. 227–264.

Şengör, A. C., C. Zabcı, and B. A. Natal'in, 2019, “Continental transform faults: congruence and incongruence with normal plate kinematics”, In *Transform plate boundaries and fracture zones*, Vol. 9, pp. 169-247.

Tan, O., 2021, “A homogeneous earthquake catalogue for Turkey”, *Natural Hazards and Earth System Sciences*, Vol. 21, No. 7, pp. 2059-2073.

Tavakoli, F., F. Nilforoushan, A. Walpersdorf, M. Tatar, Y. Djamour, H. Nankali, J. F. Ritz, P. Vernant, 2008, “Distribution of the right-lateral strike-slip motion from the Main Recent Fault to the Kazerun Fault System (Zagros, Iran): evidence from present-day GPS velocities”, *Earth and Planetary Science Letters*, Vol. 275, No. 3–4, pp. 342–347.

Tinti, S., and F. Mulargia, 1985, “An improved method for the analysis of the completeness of a seismic catalogue”, *Lettere al Nuovo Cimento (1971-1985)*, Vol. 42, No. 1, pp. 21-27.

Toda, S., R. S. Stein, K. Richards-Dinger, and S. B. Bozkurt, 2005, “Forecasting the evolution of seismicity in southern California: Animations built on earthquake stress transfer”, *Journal of Geophysical Research: Solid Earth*, Vol. 110, No. 5.

Toda, S., R. S. Stein, J. Lin, 2011, “Widespread seismicity excitation throughout central Japan following the 2011 M = 9.0 Tohoku earthquake and its interpretation by Coulomb stress transfer”, *Geophysical Research Letters*, Vol. 38, No. 7.

Türkoğlu, E., M. Unsworth, F. Bulut, and İ. Çağlar, 2015, “Crustal structure of the North Anatolian and East Anatolian Fault Systems from magnetotelluric data”, *Physics of the Earth and Planetary Interiors*, Vol. 241, pp. 1–12.

Utsu, T., 1965, “A method for determining the value of b in a formula $\log n = a - bM$ showing the magnitude–frequency relation for earthquakes”, *Geophysical Bulletin of the Hokkaido University*, Vol. 13, pp. 99–103.

Walpersdorf, A., M. Tatar, Y. Djamour, H. Nankali, J. F. Ritz, F. Nilforoushan, F. Tavakoli, A. Ashtiani, 2006, “Difference in the GPS deformation pattern of North and Central Zagros (Iran)”, *Geophysical Journal International*, Vol. 167, No. 3, pp. 1077–1088.

Walpersdorf, A., H. Nankali, Y. Djamour, F. Nilforoushan, F. Tavakoli, M. Tatar, S. Van Gorp, P. Vernant, F. Masson, 2014, “Present-day kinematics and fault slip rates in

Eastern Iran, derived from 11 years of GPS data", *Journal of Geophysical Research*, Vol. 119, No. 2, pp. 1359–1383.

Westerhaus, M., M. Wyss, R. Yilmaz, and J. Zschau, 2002, "Correlating variations of b values and crustal deformations during the 1990s may have pinpointed the rupture initiation of the M w= 7.4 Izmit earthquake of 1999 August 17", *Geophysical Journal International*, Vol. 148, No. 1, pp. 139-152.

Wiemer, S., and M. Wyss, 1997, "Mapping the frequency–magnitude distribution in asperities: An improved technique to calculate recurrence times?", *Journal of Geophysical Research: Solid Earth,* Vol. 102, No. B7, pp. 15115–15128.

Wiemer, S., 2001, "A software package to analyze seismicity: ZMAP", *Seismological Research Letters*, Vol. 72, No. 3, pp. 373-382.

Wiemer, S., and M. Wyss, 2000, "Minimum magnitude of completeness in earthquake catalogs: Examples from Alaska, the western United States, and Japan", *Bulletin of the seismological society of America*, Vol. 90, No. 4, pp. 859-869.

Woessner, J., and S. Wiemer, 2005, "Assessing the quality of earthquake catalogues: Estimating the magnitude of completeness and its uncertainty", *Bulletin of the Seismological Society of America*, Vol. 95, No. 2, pp. 684-698.

Wyss, M., 1973, "Towards a physical understanding of the earthquake frequency distribution", *Geophysical Journal of the Royal Astronomical Society,* Vol. 31, No. 4, pp. 341–359.

Wyss, M., and W. H. Lee, 1973, "Time variations of the average earthquake magnitude in central California", *Proceedings of the Conference on Tectonic Problems of the San Andreas Fault System*. pp. 24–42.

Yıldız, S. S., A. Özkan, H. Yavaşoğlu, F. Masson, İ. Tiryakioğlu, M. N. Alkan, and S. Bilgi, 2020, "Determination of recent tectonic deformations in the vicinity of Adana–

Osmaniye–Hatay–Gaziantep triple junction region by half-space modeling”, *Comptes Rendus. Géoscience*, Vol. 352, No. 3, pp. 225–234.

Yılmaz, H., S. Över, and S. Özden, 2006, “Kinematics of the east Anatolian Fault zone between turkoglu (Kahramanmaras) and celikhan (adiyaman), eastern Turkey”, *Earth, planets and space*, Vol. 58, No. 11, pp. 1463-1473.

Yönlü, Ö., E. Altunel, and V. Karabacak, 2017, “Geological and geomorphological evidence for the southwestern extension of the East Anatolian Fault Zone, Turkey”, *Earth and Planetary Science Letters*, Vol. 469, pp. 1-14.

Zarifi, Z., F. Nilfouroushan, and M. Raeesi, 2014, “Crustal Stress Map of Iran: insight from seismic and geodetic computations,” *Pure and Applied Geophysics*, Vol. 171, pp. 1219–1236.